Theoretical Study of Semiconductor Quantum Dot Lasers with Asymmetric Barrier Layers

John L. Monk III

Thesis submitted to the faculty of the

Virginia Polytechnic Institute and State University

in partial fulfillment of the requirements for the degree of

Master of Science

In

Materials Science and Engineering

Levon V. Asryan, Chair

Giti A. Khodaparast

William T. Reynolds

April 29th, 2020

Blacksburg, Virginia

Keywords: quantum dot lasers, semiconductor lasers

Theoretical Study of Semiconductor Quantum Dot Lasers with Asymmetric Barrier Layers

Jack Monk

ABSTRACT

Small-signal dynamic response of semiconductor quantum dot (QD) lasers with asymmetric barrier layers was studied. Semiconductor lasers are used in many communication systems. Fiber optic communication systems use semiconductor lasers in order to transmit information. DVD and Blu-ray disk players feature semiconductor lasers as their readout source. Barcode readers and laser pointers also use semiconductor lasers. A medical application of semiconductor lasers is for minor soft tissue procedures. Semiconductor lasers are also used to pump solid-state and fiber lasers. Semiconductor lasers are able to transmit telephone, internet, and television signals through fiber optic cables over long distances. The amount of information able to be transferred is directly related to the bandwidth of the laser. By introducing asymmetric barrier layers, the modulation bandwidth of the laser will improve, allowing for more information to be transferred. Also, by introducing asymmetric barrier layers, the output power will be unrestricted, meaning as more current is applied to the system, the laser will get more powerful. An optimum pumping current was found which maximized modulation bandwidth at -3dB, and is lower in QD lasers with asymmetric barrier layers (ABL) as opposed to conventional QD lasers. Modulation bandwidth was found to increase with cross section of carrier capture before reaching an asymptote. Both surface density of QDs and cavity length had optimum values which

maximized modulation bandwidth. Relative QD size fluctuation was considered in order to see how variation in QD sizes effects the modulation bandwidth of the semiconductor QD laser with ABLs. These calculations give a good starting point for fabricating semiconductor QD lasers with ABLs featuring the largest modulation bandwidth possible for fiber optic communication systems.

In semiconductor QD lasers, the electrons and holes may be captured into excited states within the QDs, rather than the ground state. The particles may also jump from the ground state up to an excited state, or drop from the excited state to the ground state. Recombination of electron-hole pairs can occur from the ground state to the ground state or from an excited state to an excited state. In the situation if the capture of charge carriers into the ground state in QDs takes place via the excited-state, then this two-step capture process makes the output power from ground-state lasing to saturate in conventional QD lasers. By using ABLs in the QD laser, it is predicted that the output power of ground-state lasing will continue to rise with applied current, as the ABLs will stop the electrons and holes from recombining in the optical confinement layer. Thus, ABL QD lasers will be able to be used in applications that require large energy outputs.

Theoretical Study of Semiconductor Quantum Dot Lasers with Asymmetric Barrier Layers

Jack Monk

GENERAL AUDIENCE ABSTRACT

Semiconductor lasers (also known as diode lasers) have been used in numerous applications ranging from communication to medical applications. Among all applications of diode lasers, of particular importance is their use for high speed transmission of information and data in fiber optic communication systems. This is accomplished by direct conversion of the diode laser input (electrical current) to its output (optical power). Direct modulation of the laser optical output through varying electrical current helps cut costs by not requiring other expensive equipment in order to perform modulation.

The performance of conventional semiconductor lasers suffers from parasitic recombination outside of the active region – an unwanted process that consumes a considerable fraction of the laser input (injection current) while not contributing to the useful output and thus damaging its performance.

Asymmetric barrier layers were proposed as a way to suppress parasitic recombination in semiconductor lasers. In this study, the optimal conditions for semiconductor quantum dot lasers with asymmetric barrier layers were calculated in order to maximize their modulation bandwidth – the parameter that determines the highest speed of efficient information transmission. This

includes finding the optimal values of the dc component of the pump current, quantum dot surface density and size fluctuations, and cavity length. As compared to conventional quantum dot lasers, the optimal dc current maximizing the modulation bandwidth is shown to be considerably lower in quantum dot lasers with asymmetric barrier layers thus proving their outperforming efficiency.

In the presence of extra states in quantum dots in conventional lasers, the optical output of needed ground-state lasing may be heavily impacted – it may remain almost unchanged with increasing the laser input current. As opposed to conventional lasers, the output power of ground-state lasing in devices with asymmetric barrier layers will continue growing as more input current is applied to the system.

Acknowledgments

I would like to give a sincere thank you to the following individuals for their support and encouragement throughout my Ph.D. course:

- My wonderful advisor, Dr. Levon Asryan, for all his guidance and support throughout my time working with him. No words would adequately describe his influence both professionally and personally, so I will simply say thank you.
- Dr. Giti Khodaparast and Dr. William Reynolds for taking the time to be on my committee. Their courses and guidance have proven instrumental in extending my knowledge in both physics and materials science.

I would like to thank the United States Army Research Office (Grant No. W911NF-17-1-0432) for funding this work.

I would also like to thank all the members of the MSE Department and my friends that I have made during my time at Virginia Tech. None of this would have happened without you all.

I would of course like to thank my fiancé, Samantha Drewry, for her love, patience, encouragement, and understanding. I look forward to many more adventures with you.

I would be amiss to not thank my wonderful mother, grandmother, and sister; whose love, support, encouragement and belief have never failed.

I would finally like to thank my grandfather, John L Monk Sr., and my father John L. Monk Jr. I have looked up to you both all my life, and would not be the man I am today without you both. I am proud to be the third.

Table of Contents

List of Figures

Chapter 1. Introduction

Semiconductor lasers, also known as laser diodes or diode lasers, are used for a variety of applications, such as laser printers, bar-code readers, and laser pointers. Semiconductor lasers use p-n junctions, commonly used in semiconductor devices, to achieve lasing. Semiconductor lasers feature direct modulation through a varying electrical current, helping cut costs by not requiring other expensive equipment in order to perform modulation. Because of this, these lasers are also used in high-speed fiber optic communication systems as transmitters that are able to convert input electrical signal to output optical signal.

The ability to control the semiconductor material conductivity through doping with various impurities and the carrier injection opened the doors to semiconductor electronics development.

Heterostructure development allowed the control of fundamental parameters within semiconductor devices and crystals, including band gaps and refractive indices. Semiconductor heterostructure based devices include laser-based communication systems and light-emitting diodes (LED's).

Semiconductor lasers operate using stimulated emission, where one incoming photon stimulates the emission of a second photon through recombination of an electron-hole pair. Figure 1 shows a schematic of the interaction between light and matter. When an incident photon enters a semiconductor, it may be absorbed by an electron in the valence band, and excite the electron. This excited electron will then jump up into the conduction band, leaving behind a positively charged hole in its stead. Thus, the electron-hole pair is generated [Fig. 1 (a)].

Electron-hole pairs may recombine with no external influence, in a process called spontaneous emission, as shown in Fig. 1 (b). The emitted photons from spontaneous emission are at different phases with random direction. When recombination is stimulated by an incident photon [Fig 1 (c)], the emitted photon from the electron-hole recombination has the same wavelength, phase, and direction of propagation as the incident photon. This process is called stimulated emission, and emits coherent photons.

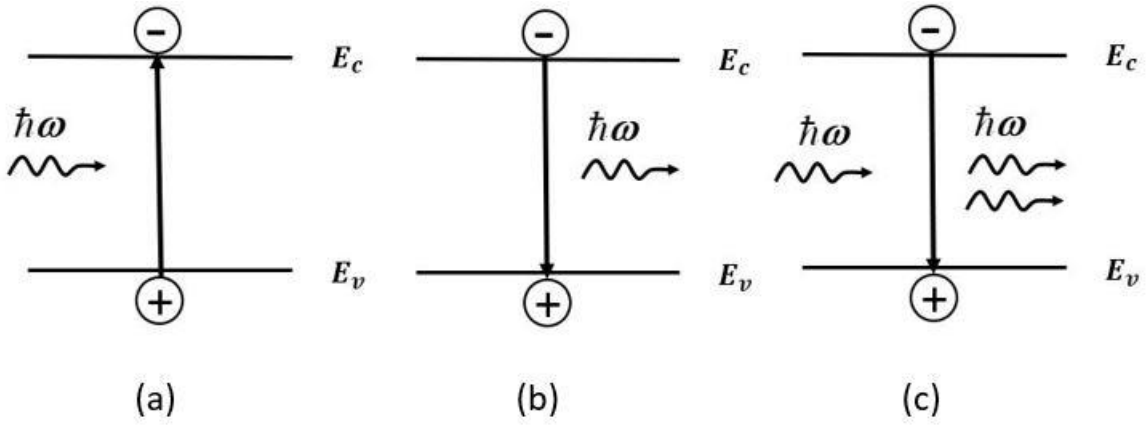

Fig. 1. Schematic illustration of (a) excitation of an electron from the valence band to the conduction band through absorption of a photon, (b) spontaneous emission of a photon, and (c) stimulated emission by an incident photon.

In semiconductors under thermal equilibrium, the electron distribution follows the Fermi-Dirac statistics and the lower energy levels are more populated than the higher energy levels of the semiconductor. Thusly, the photon absorption process is dominant and no coherent light is emitted. In order for lasing to occur, the stimulated emission of photons must overtake the photon absorption process of the semiconductor. Therefore, pumping is required to make the

upper energy level of the semiconductor more populated than the lower one, creating a population inversion. This allows the optical gain and amplification of electro-magnetic radiation to be established. Thus, a laser is created (Light Amplification by Stimulated Emission of Radiation).

The first studies on semiconductor lasers were performed in the early 1960s [1-3]. In 1964, the first electrically operated semiconductor laser was created by Hall [4]. Hall's design operated at 77K, and was based upon a GaAs p-n junction. Also in 1964, other groups managed to obtain lasing in semiconductor in both visible and infrared light ranges [5,6]. These homojunction structures were created using p-n junctions composing of the same semiconductor material, and featured poor lasing efficiencies and suffered additionally from high threshold current density. They also suffered from high optical and electrical loss. These early homojunction lasers were unable to achieve lasing outside of cryogenic temperatures.

In 1963, the first double-heterostructure (DHS) laser was conceptualized [7, 8]. By 1970, the first double heterostructure laser was demonstrated [9-11]. These double heterostructure lasers were shown to operate continuously at room temperature and had a lower threshold current density than previously designed homojunction lasers. Due to the separate confinement of carriers and photons in DHS lasers, the lasing threshold was lowered significantly and continuous wave operation at room temperature became possible [12]. The double heterostructures lasers also allowed the emitted surface to be enlarged and new materials to be used.

In conventional diode lasers, lasing is achieved through recombination of electrons and holes in the active region located in the center of the optical confinement layer (OCL). The OCL

confines photons emitted in the active region: due to the fact that the OCL refractive index is higher than that of the cladding layers, a waveguide is created, and confines the emitted photons within the OCL effectively.

The electrons and holes are injected into the OCL from cladding layers on opposite sides of the OCL. They are then transported into the active region, and recombine there. The electron-hole pairs that recombine in the active region output photons of a desired energy. The active region bandgap dictates the energy of the output photon.

In quantum well (QW), quantum wire (QWR), and QD lasers, the quantum-confined region is embedded into the OCL. The electrons first enter the OCL, then get captured into the active region. By using low dimensional active region, the laser performance is improved, compared with bulk laser performance. Emitted photon wavelength is tunable by changing the thickness of the low-dimensional active layer, in addition to changing the composition and material used in the active layer.

Bulk material was used in the active region of early heterostructure lasers, which allowed the carriers freedom to wander in three dimensions. This limited the operation of the laser. By shrinking the active region to a size comparable to the de Broglie wavelength of the carrier, the carrier becomes quantum confined in the active region and has a discrete energy spectrum. The classification of the laser is based on the number of degrees of freedom of the carrier in the active region: 2 (quantum well), 1 (quantum wire), or 0 (quantum dot).

Thermal spreading of carriers over multiple energy states causes the threshold current temperature dependence in bulk lasers. In QW lasers, the density of states is a step-function, shown in Fig. 3. (b) [13]. This limits thermal spreading, as opposed to bulk lasers (Fig. 3. (a)). QWR

lasers further suppress the temperature effect of thermal spreading due to the density of states taking the form of a decreasing function of energy (Fig. 3. (c)). QDs ideally cause thermal spreading of carriers to disappear, since the density of states in QDs is a delta-function, and there are no additional available states for carriers to move to through thermal spreading, as shown in Fig. 3. (d).

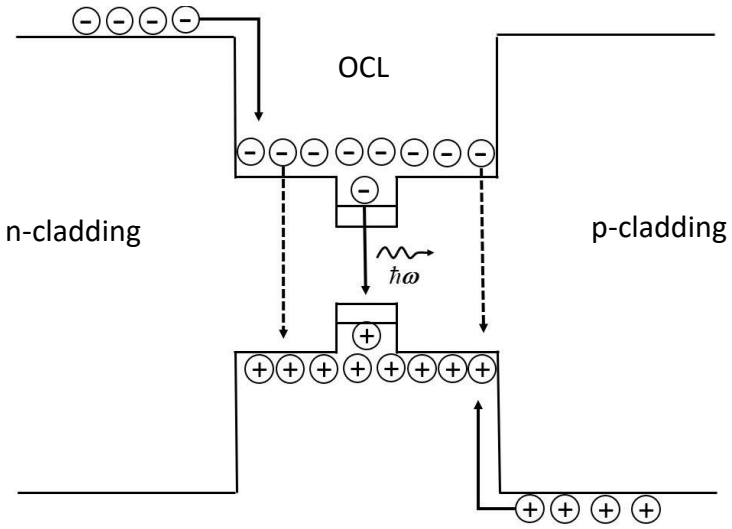

Fig. 2. A conventional quantum dot laser. Solid arrow shows recombination in the active region. Dashed arrows show recombination in the OCL (parasitic recombination).

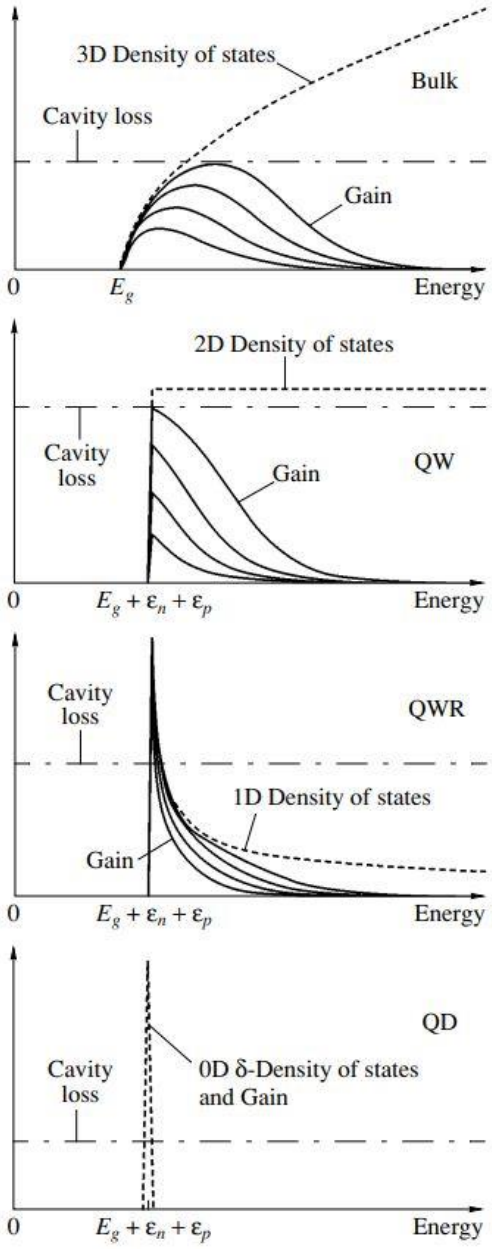

Fig. 3. Modification of the density of states and the shape of the gain spectrum with decreasing dimensionality of the active region. [13] (Reprinted by permission from Springer Nature) Springer Semiconductors L.V. Asryan and R.A. Suris, "Theory of threshold characteristics of semiconductor quantum dot lasers," Semicond., vol. 38, no. 1, pp. 1-22, Jan. 2004.

Because of the compact size and direct modulation of the emitted power through alternating electric current capabilities, semiconductor lasers are commonly used in high-speed communication systems. The semiconductor laser acts as a transmitter, converting electrical signal to optical, as shown in Figure 4. The directly-modulating bias current input signal causes the following changes in laser optical output power, and transmits information through this process. In light wave communication systems, the modulation bandwidth is the highest frequency at which the modulation continues to be efficient, which directly determines the amount of information that can be transmitted per unit time. Thus, the response of semiconductor lasers to alternating pumping current is critical for successful application in high-speed communication systems.

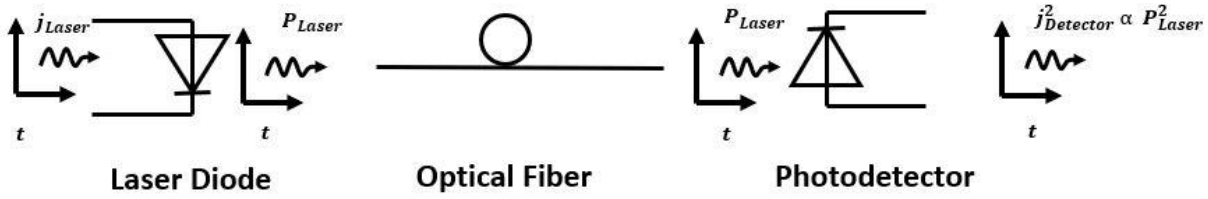

Fig. 4. Schematic diagram of a basic optical fiber communication system.

Several factors may limit the modulation bandwidth of the semiconductor QD laser. In an ideal QD laser, all the QDs would be identical in shape and size, and the density of states would appear as a delta-function. However, when fabricating QDs, there are inherent size and shape fluctuations, which can alter the QDs behaviors [14]. The size fluctuations lead to varying energies of electrons and holes, which leads to inhomogeneous broadening of the gain spectrum and to

the maximum modal gain decrease [15]. At a certain maximum inhomogeneous broadening, the lasing is no longer achievable in QD lasers [15]; the modulation bandwidth is zero at this point.

While carrier capture into the quantum-confined active region should be ideally instantaneous, in reality it is not instantaneous [15-17]. Because stimulated emission is produced by the carriers confined in QDs, the carrier capture cross-section applies a massive effect on the QD laser dynamics. In conventional semiconductor QD lasers, the carrier capture delay from the OCL into the QDs largely reduces the laser modulation bandwidth.

In conventional lasers, electrons can easily go beyond the active region and end up in the OCL on the side where the holes entered the system. Holes mirror the electrons, and will also escape the active region into the OCL on the opposite side of the active region. Electron-hole pairs that recombine in the OCL outside the active region also output a photon, but of an undesired wavelength. This is called parasitic electron-hole recombination, and is detrimental to the laser characteristics of the system, sapping power and introducing noise in the optical output signal. This is shown as the dashed arrows in Fig 2.

Asymmetric barrier layers (ABLs) were proposed [18,19] as a way to suppress parasitic recombination in semiconductor lasers, and are shown in figure 5. Asymmetric barrier layers feature a shorter wall before electrons (holes) enter the active region, and a much taller wall after the active region. This assures that the electrons, and thusly the holes, will be unable to escape the active region and cause parasitic recombination in the OCL to occur. In [20], a theoretical model for the threshold and power characteristics of ABL QD lasers was developed.

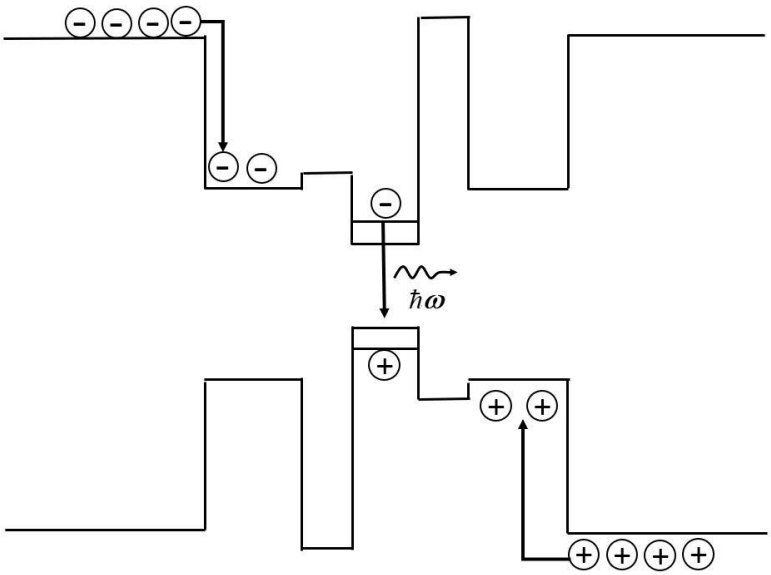

Fig. 5. Quantum dot laser with asymmetric barrier layers.

In this work, a semiconductor QD laser with ABLs was modeled, and the effects of applied current, carrier capture cross section, and the parameters of the laser structure were investigated with regards to modulation bandwidth. The effects of relative QD size fluctuation on modulation bandwidth was also investigated.

Ideally, only one electron (and hole) energy level should exist in a QD. In actual QDs containing excited states in addition to the ground state, it is possible for a carrier to be captured into an excited state, rather than the ground state. Should the carrier capture into the QD ground-state be excited-state-mediated, the ground-state lasing power will eventually reach an asymptotic value rather than continues to increase with increasing pump current in a conventional QD lasers. In this study, QD lasers with ABLs were modeled to investigate how ABLs effect the output power of ground-state lasing in the case of the carrier capture into the QD ground-state again being excited-state-mediated.

While there has been no experimental work on QD lasers with ABLs so far, there is an ongoing experimental and theoretical activity on QW lasers with ABLs.

In [21, 22], a QW laser with ABLs was fabricated for the first time. The QW material was GaAs and the OCL material was $Al_{0.2}Ga_{0.8}As$. The lasing wavelength was 835.6 nm. The material of the ABL on the n-side of the structure was $Ga_{0.55}In_{0.45}P$ and that on the p-side – $Al_{0.42}Ga_{0.36}In_{0.22}As$. Already in this first experimental ABL QW laser, a reduced and less temperature-sensitive threshold current was achieved as compared to a reference QW laser (a laser without ABLs that was otherwise similar to the laser with the ABLs).

In [23, 24], for the ABL QW laser of the same material composition as in [21, 22, 25], improved power characteristics were observed as compared to a reference structure: the light-current characteristic was more linear, the slope and wall-plug efficiencies were higher, and the maximum output optical power was obtained at a lower pump current.

In [26], using the method of scanning near-field optical microscopy, it was directly observed that the luminescence associated with the parasitic recombination in the OCL was less intense in the ABL QW laser as compared to the reference laser.

It is assumed in this study that the ABLs function ideally, i.e., the ABL on the n-side of the OCL completely blocks the hole transport (both by tunneling and over the barrier) to that side of the structure while not affecting the electron injection into the QDs. Similarly, the ABL on the p-side of the OCL is assumed to completely block the electron transport (both by tunneling and over the barrier) to that side of the structure while not affecting the hole injection into the QDs. It should be noted here that a rigorous study of the candidate materials for the ABLs will be needed for a proper design of experimental QD lasers with ABLs blocking the transport of foreign

carriers to an extent that will be sufficient for a considerable suppression of the parasitic recombination in the OCL. That study should particularly focus on the search for the materials compositions providing a low conduction band offset and a high valence band offset on the n-side of the structure and a low valence band offset and a high conduction band offset on the p-side. That study is beyond the scope of this work. For QW lasers with the ABLs, such a study has been performed in [27]–[30].

The present-day commercial diode lasers use QWs as their active region. Despite the fact that there has been a remarkable progress in fabricating QD lasers (the progress was largely made possible with the use of the self-assembly technique (the Stranski-Krastanov growth mode) for forming QDs [14, 31, 32]), the conventional QD lasers have not yet superseded the QW lasers in large-scale commercial applications. The QD lasers with properly designed ABLs (so that the parasitic recombination in their OCL is significantly suppressed) possess major advantages both over the conventional QD and QW lasers and hence are a viable candidate for their replacement.

Manuscript in Preparation

[1] J. L. Monk and L. V. Asryan, "Small-signal modulation bandwidth of quantum-dot lasers with asymmetric barrier layers."

Presentation at Conferences

[1] L. V. Asryan and J. L. Monk, "Small-signal dynamic response of quantum-dot lasers with asymmetric barrier layers," International Conf. "SPIE Photonics West", San Francisco, USA, Feb. 4, 2020. Paper no. 11274-25.

Presentation at the seminars at the Department of Materials Science and Engineering at Virginia Polytechnic Institute and State University

[1] J. L. Monk and L. V. Asryan, "Semiconductor quantum dot lasers with asymmetric barrier layers," Oct. 18, 2019.

Chapter 1 Bibliography

[1] N. G. Basov, B. M. Vul and Y. M. Popov, "Quantum-mechanical semiconductor generators and amplifiers of electromagnetic oscillations," Sov. Phys. JETP, vol. 10, pp. 416, 1960.

[2] W. S. Boyle and D. G. Tomas, "Optical maser," U.S. Patent 3 059 117, Oct. 16, 1962.

[3] N. G. Basov, O. N. Krokhin and Y. M. Popov, "Production of negative-temperature states in p-n junctions of degenerate semiconductors," Sov. Phys. JETP, vol. 13, pp. 1320-1321, 1961.

[4] R. N. Hall, G. E. Fenner, J. D. Kingsley, T. J. Soltys and R. O. Carlson, "Coherent Light Emission From GaAs Junctions," Phys. Rev. Lett., vol. 9, no. 9, pp. 366-368, Nov. 1962.

[5] J. N. Holonyak and S. F. Bevacqua, "Coherent (visible) light emission from Ga(As1-xPx) junctions," Appl. Phys. Lett., vol. 1, no. 4, pp. 82-83, Dec. 1962.

[6] M. I. Nathan, W. P. Dumke, G. Burns, J. F. H. Dill and G. Lasher, "Stimulated emission of radiation from GaAs p-n junctions," Appl. Phys. Lett., vol. 1, no. 3, pp. 62-64, Nov. 1962.

[7] Zh. I. Alferov and R. F. Kazarinov, "Semiconductor laser with electric pumping," USSR Patent 181737, Mar. 30, 1963.

[8] H. Kroemer, "Solid state radiation emitters," U.S. Patent 3 309 553, Aug. 16, 1963.

[9] Zh. I. Alferov, V. M. Andreev, D. Z. Garbuzov, Yu. V. Zhilyaev, E. P. Morozov, E. L. Portnoi and V. G. Trofim, "Investigation of influence of AlAs-GaAs heterostructure parameters on laser

threshold current and realization of continuous emission at room temperature," Fiz. Tekh. Poluprovodn., vol. 4, no. 9, pp. 1826-1829, 1970.

[10] I. Hayashi, M. B. Panish, P. W. Foy and S. Sumski, "Junction lasers which operate continuously at room temperature," Appl. Phys. Lett., vol. 17, no. 3, pp. 109-111, Aug. 1970.

[11] M. B. Panish, I. Hayashi and S. Sumski, "Double-heterostructure injection lasers with roomtemperature thresholds as low as 2300 A/cm2," Appl. Phys. Lett., vol. 16, no. 8, pp. 326-327, Apr. 1970.

[12] Zh. I. Alferov, "Nobel Lecture: The double heterostructure concept and its applications in physics, electronics, and technology," Reviews of Modern Physics, vol. 73, no. 3, pp. 767-782, July 2001.

[13] L.V. Asryan and R.A. Suris, "Theory of threshold characteristics of semiconductor quantum dot lasers," Semicond., vol. 38, no. 1, pp. 1-22, Jan. 2004.

[14] D. Leonard, S. Fafard, K. Pond, Y. H. Zhang, J. L. Merz and P. M. Petroff, "Structural and Optical-Properties of Self-Assembled InGaAs Quantum Dots," J Vac Sci Technol B, vol. 12, no. 4, pp. 2516-2520, Jul./Aug. 1994.

[15] L. V. Asryan and R. A. Suris, "Inhomogeneous line broadening and the threshold current density of a semiconductor quantum dot laser," Semicond. Sci. Technol., vol. 11, no. 4, pp. 554-567, Apr. 1996.

[16] L. V. Asryan, S. Luryi and R. A. Suris, "Intrinsic nonlinearity of the light-current characteristic of semiconductor lasers with a quantum-confined active region," Appl. Phys. Lett., vol. 81, no. 12, pp. 2154-2156, Sept. 2002.

[17] L. V. Asryan, S. Luryi and R. A. Suris, "Internal efficiency of semiconductor lasers with a quantum-confined active region," IEEE J. Quantum. Electron., vol. 39, no. 3, pp. 404-418, Mar. 2003.

[18] L.V. Asryan and S. Luryi, "Temperature-insensitive semiconductor quantum dot laser," Solid-State Electron., vol. 47, no. 2, pp. 205-212, Feb. 2003.

[19] L.V. Asryan and S. Luryi, "Semiconductor laser with reduced temperature sensitivity," U.S. Patent No. 6,870,178, Mar. 22, 2005

[20] L. V. Asryan, "Quantum dot lasers with asymmetric barrier layers: Close-to-ideal threshold and power characteristics," Quantum Electron., vol. 49, no. 6, pp. 522-528, June 2019.

[21] A.E. Zhukov, N.V. Kryzhanovskaya, F.I. Zubov, Y.M. Shernyakov, M.V. Maximov, E.S. Semenova, K. Yvind, and L.V. Asryan, “Improvement of temperature-stability in a quantum well laser with asymmetric barrier layers,” Appl. Phys. Lett., vol. 100, no. 2, Art. no. 021107, Jan. 2012.

[22] A.E. Zhukov, L.V. Asryan, Yu.M. Shernyakov, M.V. Maximov, F.I. Zubov, N.V. Kryzhanovskaya, K. Yvind, and E.S. Semenova, “Effect of asymmetric barrier layers in the waveguide region on the temperature characteristics of quantum-well lasers,” Semicond., vol. 46, no. 8, pp. 1027-1031, Aug. 2012.

[23] F.I. Zubov, A.E. Zhukov, Yu.M. Shernyakov, M.V. Maximov, N.V. Kryzhanovskaya, K. Yvind, E.S. Semenova, and L.V. Asryan, “The effect of asymmetric barrier layers in the waveguide region on power characteristics of QW lasers,” Technical Phys. Lett., vol. 41, no. 5, pp. 439-442, May 2015.

[24] F.I. Zubov, M.V. Maximov, Yu.M. Shernyakov, N.V. Kryzhanovskaya, E.S. Semenova, K. Yvind,

L.V. Asryan, and A.E. Zhukov, “Suppression of sublinearity of light–current curve in 850 nm quantum well laser with asymmetric barrier layers,” Electron. Lett., vol. 51, no. 14, pp. 1106-1108, July 2015.

[25] F.I. Zubov, A.E. Zhukov, Yu.M. Shernyakov, M.V. Maximov, E.S. Semenova, and L.V. Asryan, “Diode lasers with asymmetric barriers for 850 nm spectral range: experimental studies of power characteristics,” J. Phys. Conf. Ser., vol. 643, Art. no. 012042, Nov. 2015.

[26] Yu.S. Polubavkina, F.I. Zubov, E.I. Moiseev, N.V. Kryzhanovskaya, M.V. Maximov, E.S. Semenova, K. Yvind, L.V. Asryan, and A.E. Zhukov, “Specific features of waveguide recombination in laser structures with asymmetric barrier layers,” Semicond., vol. 51, no. 2, pp. 254-259, Feb. 2017.

[27] L.V. Asryan, N.V. Kryzhanovskaya, M.V. Maximov, A.Yu. Egorov, and A.E. Zhukov, "Bandedge-engineered quantum well laser," Semicond. Sci. Technol., vol. 26, no. 5, Art. no. 055025, 8 pages, May 2011.

[28] F.I. Zubov, M.E. Muretova, L.V. Asryan, E.S. Semenova, M.V. Maximov, and A.E. Zhukov, “Feasibility study for Al-free 808 nm lasers with asymmetric barriers suppressing waveguide recombination,” J. Appl. Phys., vol. 124, no. 13, Art. no. 133105, 8 pages, Oct. 2018.

[29] F.I. Zubov, M.E. Muretova, L.V. Asryan, E.S. Semenova, M.V. Maximov, V.V. Korenev, A.V. Savelyev, and A.E. Zhukov, “A search for asymmetric barrier layers for 1550 nm Al-free diode lasers,” Semicond., vol. 52, no. 14, pp. 1905-1908, Dec. 2018.

[30] F.I. Zubov, M.E. Muretova, A.S. Payusov, M.V. Maximov, A.E. Zhukov, and L.V. Asryan, “Parasitic recombination in a laser with asymmetric barrier layers,” Semicond., vol. 54, no. 3, pp. 296-303, Mar. 2020.

[31] A.Yu. Egorov, A. E. Zhukov, P. S. Kop'ev, N. N. Ledentsov, M. V. Maksimov, and V. M. Ustinov, "Effect of deposition conditions on the formation of (In,Ga)As quantum clusters in a GaAs matrix," Semicond., vol. 28, no. 8, pp. 809-811, Aug. 1994.

[32] G. T. Liu, A. Stintz, H. Li, K. J. Malloy, and L. F. Lester, "Extremely low room-temperature threshold current density diode lasers using InAs dots in $In_{0.15}Ga_{0.85}As$ quantum well," Electron. Lett., vol. 35, no. 14, pp. 1163–1165, Jul. 1999.

Chapter 2. Modulation Bandwidth of Semiconductor Quantum Dot Lasers with Asymmetric Barrier Lasers.

By modifying the conduction and valence bandedges of the semiconductor QD laser, asymmetric barrier layers can be created on each side of the active region (Fig.5). These will prevent electrons and holes from escaping the active region and entering the wrong side of the OCL. We assume that the asymmetric barrier layers are ideal, such that the left-hand ABL denies holes from entering the left-hand side of the OCL and the right-hand side ABL denies electrons from entering the right-hand side of the OCL. This is all done while not hindering the injection of electrons and holes into the QDs.

2.1. Theoretical Model: Rate Equations

The theoretical model is based on the following rate equations:

for electrons in the left hand side of the OCL,

$$b_1 \frac{\partial n_{\mathrm{L}}}{\partial t} = \frac{j}{e} + \sigma_{\mathrm{n}} \mathrm{v}_{\mathrm{n}} n_1 N_{\mathrm{S}} f_{\mathrm{n}} - \sigma_{\mathrm{n}} \mathrm{v}_{\mathrm{n}} n_{\mathrm{L}} N_{\mathrm{S}} (1 - f_{\mathrm{n}}), \tag{1}$$

for holes in the right hand side of the OCL,

$$b_2 \frac{\partial p_{\mathrm{R}}}{\partial t} = \frac{j}{e} + \sigma_{\mathrm{p}} \mathrm{v}_{\mathrm{p}} p_1 N_{\mathrm{S}} f_{\mathrm{p}} - \sigma_{\mathrm{p}} \mathrm{v}_{\mathrm{p}} p_{\mathrm{R}} N_{\mathrm{S}} (1 - f_{\mathrm{p}}), \tag{2}$$

for electrons and holes confined in the QDs,

$$2N_{\mathrm{S}} \frac{\partial f_{\mathrm{n}}}{\partial t} = \sigma_{\mathrm{n}} \mathrm{v}_{\mathrm{n}} n_{\mathrm{L}} N_{\mathrm{S}} (1 - f_{\mathrm{n}}) - \sigma_{\mathrm{n}} \mathrm{v}_{\mathrm{n}} n_1 N_{\mathrm{S}} f_{\mathrm{n}} - N_{\mathrm{S}} \frac{f_{\mathrm{n}} f_{\mathrm{p}}}{\tau_{\mathrm{QD}}} - c_{\mathrm{g}} g^{\max} (f_{\mathrm{n}} + f_{\mathrm{p}} - 1) n_{\mathrm{ph}}, \tag{3}$$

$$2N_{\mathrm{S}} \frac{\partial f_{\mathrm{p}}}{\partial t} = \sigma_{\mathrm{p}} \mathrm{v}_{\mathrm{p}} p_{\mathrm{R}} N_{\mathrm{S}} (1 - f_{\mathrm{p}}) - \sigma_{\mathrm{p}} \mathrm{v}_{\mathrm{p}} p_1 N_{\mathrm{S}} f_{\mathrm{p}} - N_{\mathrm{S}} \frac{f_{\mathrm{n}} f_{\mathrm{p}}}{\tau_{\mathrm{QD}}} - c_{\mathrm{g}} g^{\max} (f_{\mathrm{n}} + f_{\mathrm{p}} - 1) n_{\mathrm{ph}}, \tag{4}$$

and for output photons,

$$\frac{\partial n_{\mathrm{ph}}}{\partial t} = c_{\mathrm{g}} g^{\max}(f_{\mathrm{n}} + f_{\mathrm{p}} - 1) n_{\mathrm{ph}} - c_{\mathrm{g}} \beta n_{\mathrm{ph}} . \tag{5}$$

For equations (1)-(5), b_1 (b_2) is the thickness of the left (right) hand side of the OCL [the separation between the n- (p-) cladding layer and the left (right) hand side barrier]. n_L and p_R are the free-electron and -hole densities. j is the injection current density, e is the electron charge, and $\sigma_{\mathrm{n,p}}$ are the cross-sections of electron and hole capture into a QD. $v_{\mathrm{n,p}}$ are the electron and hole thermal velocities, N_{S} is the surface density of QDs, $f_{\mathrm{n,p}}$ are the electron- and hole-level occupancies in QDs, τ_{QD} is the spontaneous radiative lifetime in QDs, while c_{g} is the group velocity of light in the cavity. $g^{\max}$ is the maximum value of the modal gain [15].

$$\beta = (1/L)\ln(1/R) \tag{6}$$

β is the mirror loss coefficient, L is the cavity length, R is the facet reflectivity, and n_{ph} is the photon density (number of photons per unit area of the junction).

The maximum value of the modal gain in a QD laser is [15]

$$g^{\max} = \frac{\xi}{4}\left(\frac{\lambda_0}{\sqrt{\epsilon_g}}\right)^2 \frac{1}{\tau_{\mathrm{QD}}} \frac{\hbar}{(\Delta\varepsilon)_{\mathrm{inhom}}} \frac{\Gamma}{a} N_{\mathrm{S}} , \tag{7}$$

where $\xi = 1/\pi$ and $\xi = 1/\sqrt{2\pi}$ for the Lorentzian and Gaussian QD-size distributions, respectively, λ_0 is the lasing wavelength, $\sqrt{\epsilon_g}$ is the group index of the dispersive OCL material, a is the mean size of QDs, and Γ is the optical confinement factor in a QD layer.

Inhomogeneous line broadening caused by fluctuations in QD size is as follows:

$$(\Delta\varepsilon)_{\mathrm{inhom}} = (q_{\mathrm{n}}\varepsilon_{\mathrm{n}} + q_{\mathrm{p}}\varepsilon_{\mathrm{p}})\,\delta , \tag{8}$$

where $\varepsilon_{n,p}$ are the energy levels of an electron and a hole in a mean-sized QD, $q_{n,p} = -(\partial \ln \varepsilon_{n,p} / \partial \ln a)$, and δ is the root mean square of relative QD-size fluctuations.

n_1 and p_1 in (1)–(4) characterize the intensities of electron and hole thermal escape from a QD to the OCL, and are given by

$$n_1 = N_c^{3D} \exp\left(-\frac{E_n}{T}\right), \qquad p_1 = N_v^{3D} \exp\left(-\frac{E_p}{T}\right), \tag{9}$$

where

$$N_{c,v}^{3D} = 2\left(\frac{m_{c,v}^{OCL} T}{2\pi\hbar^2}\right)^{3/2} \tag{10}$$

are the densities of states in the valence and conduction bands in the OCL, $m_{c,v}^{OCL}$ are the electron and hole effective masses in the OCL, $E_{n,p}$ are electron and hole excitation energies from a QD to the OCL, and T is the temperature (in energy units).

The first term in the right-hand side of eqn. (1) is the electron injection flux from the n-cladding layer in the OCL in units of $cm^{-2}s^{-1}$. The following term is the flux of thermal escape of electrons from the QDs to the OCL. The third and final term on the right-hand side of eqn (1) is the flux of electron capture from the OCL into the QDs.

The first term in the right-hand side of eqn. (2) is the hole injection flux from the p-cladding layer into the OCL. The following term is the flux of thermal escape of holes from QDs to the OCL. The third and final term on the right-hand of eqn. (2) is the flux of electron capture from the OCL into the QDs.

In (3) and (4), $N_S f_n f_p / \tau_{QD}$ is the spontaneous radiative recombination flux in QDs and $c_g g^{max} (f_n + f_p - 1) n_{ph}$ is the stimulated radiative recombination flux in QDs.

The first term in the right-hand side of eqn. (5) is the rate of stimulated emission of photons in units of s^{-1}. The second term is the rate of escape of photons from the cavity through the mirrors.

2.2. Electron-Hole Symmetry

In this research, electron-hole symmetry was assumed. Thus, the following three rate equations are followed, instead of eqs. (1)-(5):

for free carriers in one side of the OCL (for definiteness, for electrons in the left-hand side of the OCL),

$$b_1 \frac{\partial n_{\mathrm{L}}}{\partial t} = \frac{j}{e} + \sigma_{\mathrm{n}} \mathrm{v}_{\mathrm{n}} n_1 N_{\mathrm{S}} f_{\mathrm{n}} - \sigma_{\mathrm{n}} \mathrm{v}_{\mathrm{n}} n_{\mathrm{L}} N_{\mathrm{S}} (1 - f_{\mathrm{n}}) , \tag{11}$$

for carriers confined in QDs,

$$2N_{\mathrm{S}} \frac{\partial f_{\mathrm{n}}}{\partial t} = \sigma_{\mathrm{n}} \mathrm{v}_{\mathrm{n}} n_{\mathrm{L}} N_{\mathrm{S}} (1 - f_{\mathrm{n}}) - \sigma_{\mathrm{n}} \mathrm{v}_{\mathrm{n}} n_1 N_{\mathrm{S}} f_{\mathrm{n}} - N_{\mathrm{S}} \frac{f_{\mathrm{n}}^2}{\tau_{\mathrm{QD}}} - c_{\mathrm{g}} g^{\max} (2 f_{\mathrm{n}} - 1) n_{\mathrm{ph}} , \tag{12}$$

and for photons,

$$\frac{\partial n_{\mathrm{ph}}}{\partial t} = c_{\mathrm{g}} g^{\max} (2 f_{\mathrm{n}} - 1) n_{\mathrm{ph}} - c_{\mathrm{g}} \beta n_{\mathrm{ph}} . \tag{13}$$

2.2.1. Steady-State Solutions of (11)-(13)

Adding up eqs. (11) and (12), we will obtain

$$\frac{\partial}{\partial t} (b_1 n_{\mathrm{L}} + 2N_{\mathrm{S}} f_{\mathrm{n}}) = \frac{j}{e} - N_{\mathrm{S}} \frac{f_{\mathrm{n}}^2}{\tau_{\mathrm{QD}}} - c_{\mathrm{g}} g^{\max} (2 f_{\mathrm{n}} - 1) n_{\mathrm{ph}} . \tag{14}$$

From (14), we have

$$n_{\mathrm{L}} = n_1 \frac{f_{\mathrm{n}}}{1-f_{\mathrm{n}}} + \frac{1}{\sigma_{\mathrm{n}} \mathrm{v}_{\mathrm{n}} N_{\mathrm{S}} (1-f_{\mathrm{n}})} \left(\frac{j}{e} - b_1 \frac{\partial n_{\mathrm{L}}}{\partial t} \right). \quad (15)$$

By putting $\frac{\partial}{\partial t}$ to 0 in equations (11)-(13), the dc (steady state) quantities of $n_{L,0}$ $f_{n,0}$ and $n_{ph,0}$ were found from the following steady-state equations:

$$0 = \frac{j_0}{e} + \sigma_n v_n n_1 N_s f_{n,0} - \sigma_n v_n n_{L,0} N_s (1 - f_{n,0}) \quad (16)$$

$$0 = \sigma_n v_n n_{L,0} N_s \left(1 - f_{n,0}\right) - \sigma_n v_n n_1 N_s f_{n,0} - N_s \frac{f_{n0}^2}{\tau_{QD}} - c_g g^{max} \left(2 f_{n,0} - 1\right) n_{ph,0} \quad (17)$$

$$0 = c_g g^{max} \left(2 f_{n,0} - 1\right) n_{ph,0} - c_g \beta n_{ph,0.} \quad (18)$$

Because $n_{ph,0}$ cannot be zero, (or there would be no lasing) we obtained from (18) the following steady-state lasing condition:

$$g^{max} \left(2 f_{n,0} - 1\right) = \beta \quad (19)$$

From (19), we found:

$$f_{n,0} = \frac{1}{2} \left(1 + \frac{\beta}{g^{max}}\right) \quad (20)$$

From (16), we were able to express $n_{L,0}$ in terms of $f_{n,0}$ as follows:

$$n_{L,0} = n_1 \frac{f_{n,0}}{1 - f_{n,0}} + \frac{j_0}{e \sigma_n v_n N_s (1 - f_{n,0})} \quad (21)$$

By combining equations (16) and (17), we got

$$0 = \frac{j_0}{e} - N_s \frac{f_{n,0}^2}{\tau_{QD}} - c_g g^{max} \left(2 f_{n,0} - 1\right) n_{ph,0} \quad (22)$$

By using (19) and (22), we found

$$j_0 = e N_s \frac{f_{n,0}^2}{\tau_{QD}} + e c_g \beta n_{ph,0} \quad (23)$$

Introducing the photon lifetime in the cavity

$$\tau_{ph} = \frac{1}{c_g \beta} \tag{24}$$

Rewriting (23), we have

$$j_0 = eN_s \frac{f_{n,0}^2}{\tau_{QD}} + e\frac{n_{ph,0}}{\tau_{ph}} \tag{25}$$

Rearranging (25), we found for $n_{ph,0}$

$$n_{ph,0} = \tau_{ph}\left(\frac{j_0}{e} - N_s \frac{f_{n,0}^2}{\tau_{QD}}\right) \tag{26}$$

Equations (20), (21), and (26) give the steady-state (dc) values of the electron density in the left-handed side of the OCL, the electron level occupancy in QDs, and photon density respectively.

2.3. Small Signal Analysis of Rate Equations

In order to study the modulation response of ABL QD lasers, the small-signal analysis was applied to eqs. (11)-(13). The injection current density was

$$j = j_0 + (\delta j_{\mathrm{m}})\exp(i\omega t), \tag{27}$$

where j_0 is the dc component and the amplitude δj_{m} of the time-harmonic ac component is small. n_{L}, f_{n}, and n_{ph} in the rate equations (11) – (13) were in the form of

$$n_{\mathrm{L}} = n_{\mathrm{L},0} + (\delta n_{\mathrm{L-m}})\exp(i\omega t), \tag{28}$$

$$f_{\mathrm{n}} = f_{\mathrm{n},0} + (\delta f_{\mathrm{n-m}})\exp(i\omega t), \tag{29}$$

$$n_{\mathrm{ph}} = n_{\mathrm{ph},0} + (\delta n_{\mathrm{ph-m}})\exp(i\omega t), \tag{30}$$

where the dc components $n_{L,0}$, $f_{n,0}$, and $n_{ph,0}$ are the solutions of the rate equations (11)–(13) at the steady-state ($\partial/\partial t = 0$ in the left-hand side of these equations), which correspond to the dc component j_0 of the injection current density.

Using (28)-(30) in (11)-(13) a set of algebraic equations in the frequency-dependent small amplitudes δn_{L-m}, δf_{n-m}, and δn_{ph-m} was obtained. The solution yielded the modulation response function

$$H(\omega) = \left| \frac{\delta n_{\mathrm{ph-m}}(\omega)}{\delta n_{\mathrm{ph-m}}(0)} \right|^2 . \tag{31}$$

For the case of electron hole symmetry, using the expression for $H(\omega)$, the modulation bandwidth was calculated, defined as the -3dB bandwidth, where the response function has fallen to half of its dc ($\omega = 0$) value,

$$10 \log_{10} H(\omega_{-3\,\mathrm{dB}}) = -3 . \tag{32}$$

Using eqns. (28), (29), and (30) in (11)-(13), we obtained the following set of three algebraic equations in three small amplitudes δn_{L-m}, δf_{n-m}, and δn_{ph-m}:

$$\begin{pmatrix} C_{11} & C_{12} & C_{13} \\ C_{21} & C_{22} & C_{23} \\ C_{31} & C_{32} & C_{33} \end{pmatrix} \begin{pmatrix} \delta n_{\mathrm{L-m}} \\ \delta f_{\mathrm{n-m}} \\ \delta n_{\mathrm{ph-m}} \end{pmatrix} = \begin{pmatrix} \delta j_{\mathrm{m}}/e \\ 0 \\ 0 \end{pmatrix}. \tag{33}$$

In order to solve for C_{ij} eqns (11) and (12) were rewritten as

$$\frac{\partial n_L}{\partial t} = \frac{j}{e b_1} + \sigma_n v_n n_1 \frac{N_s}{b_1} f_n - \sigma_n v_n n_L \frac{N_s}{b_1}(1 - f_n), \tag{34}$$

$$\frac{\partial f_n}{\partial t} = \frac{1}{2}\sigma_n v_n n_L (1 - f_n) - \frac{1}{2}\sigma_n v_n n_1 f_n - \frac{1}{2}\frac{f_n^2}{\tau_{QD}} - \frac{1}{2} c_g \frac{g^{max}}{N_s}(2 f_n - 1) n_{ph} \tag{35}$$

respectively. By linearizing eqn. (14), using eqns. (27), (28), (29) and (11), we have

$$i\omega\delta n_{L-m} = \frac{\partial j_m}{eb_1} + \sigma_n v_n n_1 \frac{N_s}{b_1} f_{n-m} - \sigma_n v_n n_1 \frac{N_s}{b_1}(1 - f_{n,0})\delta n_{L-m} + \sigma_n v_n n_{L,0} \frac{N_s}{b_1} f_{n-m} \quad (36)$$

Eqn. (24) can be rewritten as

$$[\sigma_n v_n \frac{N_s}{b_1}(1 - f_{n,0}) + i\omega]\delta n_{L-m} - \sigma_n v_n \big(n_1 + n_{L,0}\big) \frac{N_s}{b_1} \delta f_{n-m} = \frac{\partial j_m}{eb_1} \quad (37)$$

Linearizing eqn. (35), with equations (30) and (12), we find

$$i\omega\delta f_{n-m} = \frac{1}{2}\sigma_n v_n (1 - f_{n,0})\delta n_{L-m} - \frac{1}{2}\sigma_n v_n \big(n_1 + n_{L,0}\big)\delta f_{n-m} - \frac{f_{n,0}}{\tau_{QD}}\delta f_{n-m} \quad (38)$$

$$- c_g \frac{g^{max}}{N_s} n_{ph,0}\delta f_{n-m} - \frac{1}{2} c_g \frac{g^{max}}{N_s}\big(2f_{n,0} - 1\big)\delta n_{ph-m}$$

Equation (38) can be then rewritten as

$$-\frac{1}{2}\sigma_n v_n (1 - f_{n,0})\delta n_{L-m} + \left(\frac{1}{2}\sigma_n v_n \big(n_1 + n_{L,0}\big) + \frac{f_{n,0}}{\tau_{QD}} + c_g \frac{g^{max}}{N_s} n_{ph,0} + i\omega\right)\delta f_{n-m} \quad (39)$$

$$+ \frac{1}{2} c_g \frac{g^{max}}{N_s}\big(2f_{n,0} - 1\big)\delta n_{ph-m} = 0$$

Linearizing (26) with (29) and (30), we have

$$i\omega\delta n_{ph-m} = 2c_g g^{max} n_{ph,0}\delta f_{n-m} + c_g g^{max}\big(2f_{n,0} - 1\big)\delta n_{ph-m} - c_g \beta \delta n_{ph-m} \quad (40)$$

$$-2c_g g^{max} n_{ph,0}\delta f_{n-m} + \big[c_g\{\beta - g^{max}\big(2f_{n,0} - 1\big)\} + i\omega\big]\delta n_{ph-m} = 0 \quad (41)$$

Returning to the linearization of the rate equations, we used (19) and (24) in the last term in the left-handed side of equation (39) to rewrite (39) as

$$-\frac{1}{2}\sigma_n v_n (1 - f_{n,0})\delta n_{L-m} + \left\{\frac{1}{2}\sigma_n v_n \big(n_1 + n_{L,0}\big) + \frac{f_{n,0}}{\tau_{QD}} + c_g \frac{g^{max}}{N_s} n_{ph,0} + i\omega\right\}\delta f_{n-m} \quad (42)$$

$$+ \frac{1}{2}\frac{1}{\tau_{ph}}\frac{1}{N_s}\delta n_{ph-m} = 0$$

Using equation (19) in (41), we found

$$-2c_g g^{max} n_{ph,0} \delta f_{n-m} + i\omega \delta n_{ph-m} = 0 \tag{43}$$

Equations (37), (42), and (43) fill out the set in (33). Thus, we found the coefficients $C_{i,j}$ (*i,j* = 1,2,3)

$$C_{11} = \sigma_n v_n \frac{N_s}{b_1}\left(1 - f_{n,0}\right) + i\omega \tag{44}$$

$$C_{12} = -\sigma_n v_n (n_1 + n_{L,0}) \frac{N_s}{b_1} \tag{45}$$

$$C_{13} = 0 \tag{46}$$

$$C_{21} = -\frac{1}{2}\sigma_n v_n \left(1 - f_{n,0}\right) \tag{47}$$

$$C_{22} = \frac{1}{2}\sigma_n v_n \left(n_1 + n_{L,0}\right) + \frac{f_{n,0}}{\tau_{QD}} + c_g \frac{g^{max}}{N_s} n_{ph,0} + i\omega \tag{48}$$

$$C_{23} = \frac{1}{2}\frac{1}{\tau_{ph}}\frac{1}{N_s} \tag{49}$$

$$C_{31} = 0 \tag{50}$$

$$C_{32} = -2c_g g^{max} n_{ph,0} \tag{51}$$

$$C_{33} = i\omega \tag{52}$$

Using these coefficients, we can solve for $\delta n_{ph-m}(\omega)$

$$\delta n_{ph-m}(\omega) = \frac{\begin{vmatrix} C_{11}(i\omega) & C_{12} & \frac{\delta jm}{e} \\ C_{21} & C_{22}(i\omega) & 0 \\ 0 & C_{32} & 0 \end{vmatrix}}{\begin{vmatrix} C_{11}(i\omega) & C_{12} & 0 \\ C_{21} & C_{22}(i\omega) & C_{23} \\ 0 & C_{32} & i\omega \end{vmatrix}} \tag{53}$$

Dividing $\delta n_{ph-m}(\omega)$ by $\delta n_{ph-m}(0)$, we found

$$\frac{\delta n_{ph-m}(\omega)}{\delta n_{ph-m}(0)} = \frac{\begin{vmatrix} C_{11}(i\omega) & C_{12} & \frac{\delta j_m}{e} \\ C_{21} & C_{22}(i\omega) & 0 \\ 0 & C_{32} & 0 \end{vmatrix}}{\begin{vmatrix} C_{11}(0) & C_{12} & \frac{\delta j_m}{e} \\ C_{21} & C_{22}(0) & 0 \\ 0 & C_{32} & 0 \end{vmatrix}} \frac{\begin{vmatrix} C_{11}(0) & C_{12} & 0 \\ C_{21} & C_{22}(0) & C_{23} \\ 0 & C_{32} & 0 \end{vmatrix}}{\begin{vmatrix} C_{11}(i\omega) & C_{12} & 0 \\ C_{21} & C_{22}(i\omega) & C_{23} \\ 0 & C_{32} & i\omega \end{vmatrix}} \tag{54}$$

Breaking this into 2 parts, we began with the first part of the right hand side of equation (54),

$$\frac{\begin{vmatrix} C_{11}(i\omega) & C_{12} & \frac{\delta j_m}{e} \\ C_{21} & C_{22}(i\omega) & 0 \\ 0 & C_{32} & 0 \end{vmatrix}}{\begin{vmatrix} C_{11}(0) & C_{12} & \frac{\delta j_m}{e} \\ C_{21} & C_{22}(0) & 0 \\ 0 & C_{32} & 0 \end{vmatrix}} = \frac{-C_{32}\begin{vmatrix} C_{11}(i\omega) & \frac{\delta j_m}{e} \\ C_{21} & 0 \end{vmatrix}}{-C_{32}\begin{vmatrix} C_{11}(0) & \frac{\delta j_m}{e} \\ C_{21} & 0 \end{vmatrix}} \tag{55}$$

Which simplifies into

$$\frac{C_{21}\frac{\delta j_m}{e}}{C_{21}\frac{\delta j_m}{e}} = 1 \tag{56}$$

Because the first part of equation (54) simplifies into 1, we are able to only focus on the second half of the right hand side of the equation. Thus, (54) simplifies into

$$\frac{\delta n_{ph-m}(\omega)}{\delta n_{ph-m}(0)} = \frac{\begin{vmatrix} C_{11}(0) & C_{12} & 0 \\ C_{21} & C_{22}(0) & C_{23} \\ 0 & C_{32} & 0 \end{vmatrix}}{\begin{vmatrix} C_{11}(i\omega) & C_{12} & 0 \\ C_{21} & C_{22}(i\omega) & C_{23} \\ 0 & C_{32} & i\omega \end{vmatrix}} \tag{57}$$

Splitting (57) into real and imaginary parts, we found

$$\frac{-C_{32}\begin{vmatrix} C_{11}(0) & 0 \\ C_{21} & C_{23} \end{vmatrix}}{-C_{32}\begin{vmatrix} C_{11}(i\omega) & 0 \\ C_{21} & C_{23} \end{vmatrix} + i\omega \begin{vmatrix} C_{11}(i\omega) & C_{12} \\ C_{21} & C_{22}(i\omega) \end{vmatrix}} \tag{58}$$

Which further simplifies to

$$\frac{C_{32}C_{23}C_{11}(0)}{C_{32}C_{23}C_{11}(i\omega) - i\omega[C_{11}(i\omega)C_{22}(i\omega) - C_{12}C_{21}]} \tag{59}$$

Remembering equation (31)

$$H(\omega)=\left|\frac{\delta n_{\text{ph-m}}(\omega)}{\delta n_{\text{ph-m}}(0)}\right|^2 . \tag{31}$$

ω_{-3dB} was found from the equation:

$$10log_{10}H(\omega_{-3dB})=-3 \tag{60}$$

$$H(\omega_{-3dB})=10^{-0.3} \tag{61}$$

Denoting

$$r=10^3\approx 1.995 \tag{62}$$

We have

$$H(\omega_{-3dB})=\frac{1}{r} \tag{63}$$

Equation (63) was then rewritten as

$$rH(\omega_{-3dB})=1 \tag{64}$$

$C_{11}(i\omega)$ and $C_{22}(i\omega)$ were also rewritten as

$$C_{11}(i\omega)=C_{11}(0)+i\omega \tag{65}$$

$$C_{22}(i\omega)=C_{22}(0)+i\omega \tag{66}$$

We then have

$$\frac{\delta n_{ph-m}(\omega)}{\delta n_{ph-m}(0)}=\frac{C_{32}C_{23}C_{11}(0)}{C_{32}C_{23}[C_{11}(0)+i\omega]-i\omega[[C_{11}(0)+i\omega][C_{22}(0)+i\omega]-C_{12}C_{21}]} \tag{67}$$

The denominator of (67) was rewritten as

$$C_{32}C_{23}C_{11}(0)+i\omega C_{32}C_{23}\text{-}\, i\omega\{C_{11}(0)C_{22}(0)+i\omega[C_{11}(0)+C_{22}(0)]+(i\omega)^2-C_{12}C_{21}\} \tag{68}$$

Which simplifies to

$$C_{32}C_{23}C_{11}(0) + i\omega[C_{32}C_{23} + C_{12}C_{21} - C_{11}(0)C_{22}(0)] - (i\omega)^2[C_{11}(0) + C_{22}(0)] - (i\omega)^3 \quad (69)$$

Breaking this into real and imaginary parts, we found

$$\{C_{32}C_{23}C_{11}(0) + [C_{11}(0) + C_{22}(0)]\omega^2\} + i\omega\{[C_{32}C_{23} + C_{12}C_{21} - C_{11}(0)C_{22}(0)] + \omega^2\} \quad (70)$$

Hence, we had for $\frac{\delta n_{ph-m}(\omega)}{\delta n_{ph-m}(0)}$,

$$\frac{\delta n_{ph-m}(\omega)}{\delta n_{ph-m}(0)} = \quad (71)$$

$$\frac{C_{32}C_{23}C_{11}(0)}{\{C_{32}C_{23}C_{11}(0)+[C_{11}(0)+C_{22}(0)]\omega^2\}+ i\omega\{[C_{32}C_{23}+C_{12}C_{21}-C_{11}(0)C_{22}(0)]+\omega^2\}}$$

Using (71), we found the modulation response function

$$H(\omega) = \left|\frac{\delta n_{ph-m}(\omega)}{\delta n_{ph-m}(0)}\right|^2 = \quad (72)$$

$$\frac{C_{32}^2C_{23}^2C_{11}^2(0)}{\{C_{32}C_{23}C_{11}(0)+[C_{11}(0)+C_{22}(0)]\omega^2\}^2+\omega^2\{[C_{32}C_{23}+C_{12}C_{21}-C_{11}(0)C_{22}(0)]+\omega^2\}^2}$$

With (72), we had from (64) for the modulation bandwidth ω_{-3dB}

$$\{C_{32}C_{23}C_{11}(0) + [C_{11}(0) + C_{22}(0)]\omega_{-3dB}^2\}^2 + \omega_{-3dB}^2\{[C_{32}C_{23} + C_{12}C_{21} - C_{11}(0)C_{22}(0)] + \omega_{-3dB}^2\}^2 = rC_{32}^2C_{23}^2C_{11}^2(0) \quad (73)$$

By rearranging (73), we derived the following cubic equation in terms of ω_{-3dB}^2

$$\omega_{-3dB}^6 + \{[C_{11}(0) + C_{22}(0)]^2 + 2[C_{32}C_{23} + C_{12}C_{21} - C_{11}(0)C_{22}(0)]\omega_{-3dB}^4 + \{[C_{32}C_{23} + C_{12}C_{21} - C_{11}(0)C_{22}(0)]^2 + 2C_{32}C_{23}C_{11}(0)[C_{11}(0) + C_{22}(0)]\}\omega_{-3dB}^2 - (r-1)C_{32}^2C_{23}^2C_{11}^2(0) = 0 \quad (74)$$

Equation (74) was rewritten in the form

$$\omega_{-3dB}^{6} + E_4\omega_{-3dB}^{4} + E_2\omega_{-3dB}^{2} - E_0 = 0 \tag{75}$$

where

$$E_4 = C_{11}^2(0) + C_{22}^2(0) + 2[C_{32}C_{23} + C_{12}C_{21}] \tag{76}$$

$$E_2 = [C_{32}C_{23} + C_{12}C_{21} - C_{11}(0)C_{22}(0)]^2 + 2C_{32}C_{23}C_{11}(0)[C_{11}(0) + C_{22}(0)] \tag{77}$$

$$E_0 = (r-1)C_{32}^2C_{23}^2C_{11}^2(0) \tag{78}$$

We then introduced all positive coefficients A_0, A_1, and A_2 as follows

$$A_0 = -C_{32}C_{23}C_{11}(0) \tag{79}$$

$$A_1 = C_{11}(0)C_{22}(0) - C_{32}C_{23} - C_{12}C_{21} \tag{80}$$

$$A_2 = C_{11}(0) + C_{22}(0) \tag{81}$$

Hence, we had from (79) - (81) and (44) – (52) the coefficients A_0, A_1, and A_2

$$A_0 = C_g g^{max} \frac{1}{b_1} \frac{n_{ph,0}}{\tau_{ph}} \sigma_n v_n (1 - f_{n,0}) \tag{82}$$

$$A_1 = \sigma_n v_n \frac{N_s}{b_1}\left(1 - f_{n,0}\right)\left[\frac{f_{n,0}}{\tau_{QD}} + \frac{1}{N_s}C_g g^{max} n_{ph,0}\right] + \frac{1}{N_s}C_g g^{max}\frac{n_{ph,0}}{\tau_{ph}} \tag{83}$$

$$A_2 = \sigma_n v_n \frac{N_s}{b_1}\left(1 - f_{n,0}\right) + \frac{1}{2}\sigma_n v_n\left(n_1 + n_{L,0}\right) + \frac{f_{n,0}}{\tau_{QD}} + c_g \frac{g^{max}}{N_s} n_{ph,0} \tag{84}$$

Using (82)-(84), equation (31) was rewritten as

$$H(\omega) = \frac{A_0^2}{(A_2\omega^2 - A_0)^2 + (\omega^3 - A_1\omega)^2} \tag{85}$$

With (85), we have from (64),

$$\frac{rA_0^2}{(A_2\omega_{-3dB}^2 - A_0)^2 + (\omega_{-3dB}^3 - A_1\omega_{-3dB})^2} = 1 \tag{86}$$

From (86), we have

$$\omega_{-3dB}^{6} + (A_2^2 - 2A_1)\omega_{-3dB}^{4} + (A_1^2 - 2A_0A_2)\omega_{-3dB}^{2} - (r-1)A_0^2 = 0 \quad (87)$$

Hence, for the coefficients E_4, E_2 and E_0, we have

$$E_4 = A_2^2 - 2A_1 \quad (88)$$

$$E_2 = A_1^2 - 2A_0A_2 \quad (89)$$

$$E_0 = (r-1)A_0^2 \quad (90)$$

Using A_0, A_1, and A_2 we wrote the expression (67) as follows:

$$\frac{\delta n_{ph-m}(\omega)}{\delta n_{ph-m}(0)} = \frac{A_0}{(A_0 - A_2\omega^2) + i\omega(A_1 - \omega^2)} \quad (91)$$

or

$$\frac{\delta n_{ph-m}(\omega)}{\delta n_{ph-m}(0)} = \frac{A_0}{(A_0 - A_2\omega^2) + i(A_1\omega - \omega^3)} \quad (92)$$

Chapter 2.4. Discussion of Results

Equation (75) (or, equivalently, eq. (87)) is a cubic equation in terms of ω_{-3dB}^{2}. Solving this equation, we modeled the behavior of ABL QD lasers at varying currents, and with different laser parameters, such as QD surface density, QD size fluctuation, and cavity length. The optimum conditions were classified as those which gave the maximum modulation bandwidth of the laser system.

2.4.1. Modulation Bandwidth vs DC Pump Current

The first parameter varied was the dc component of the pump current. Using eq. (75) [(87)], wherein j was varied, Figure 6 was found.

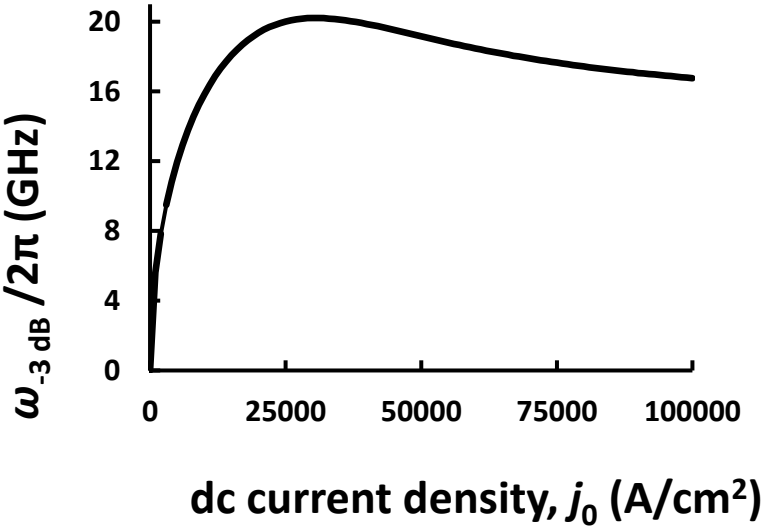

Fig. 6. $\omega_{-3dB}/2\pi$ (GHz) vs dc current density (A/cm^2).

Figure 6 clearly shows that modulation bandwidth reaches an optimum value, before falling and approaching an asymptote. The maximum value of the modulation bandwidth is 20 GHz. The optimum pump current is approximately 30 kA/cm^2. This data allows us to know the optimal pump current to operate the ABL QDL at for the largest modulation bandwidth possible. If the DC applied current is below the threshold current, lasing will not be achieved. However, if the applied current is too high, the modulation bandwidth of the ABL QDL will suffer.

Compared to optimum dc injection current of conventional QD lasers [33,34], the optimum dc injection current for ABL QD lasers is lower. Thus, the maximum bandwidth is easier to obtain in ABL QD lasers.

2.4.2. Modulation Bandwidth vs Carrier Capture Cross Section

The next parameter tested was the cross section of carrier capture. Figure 7 below shows modulation bandwidth versus current density, with varying cross sections of carrier capture.

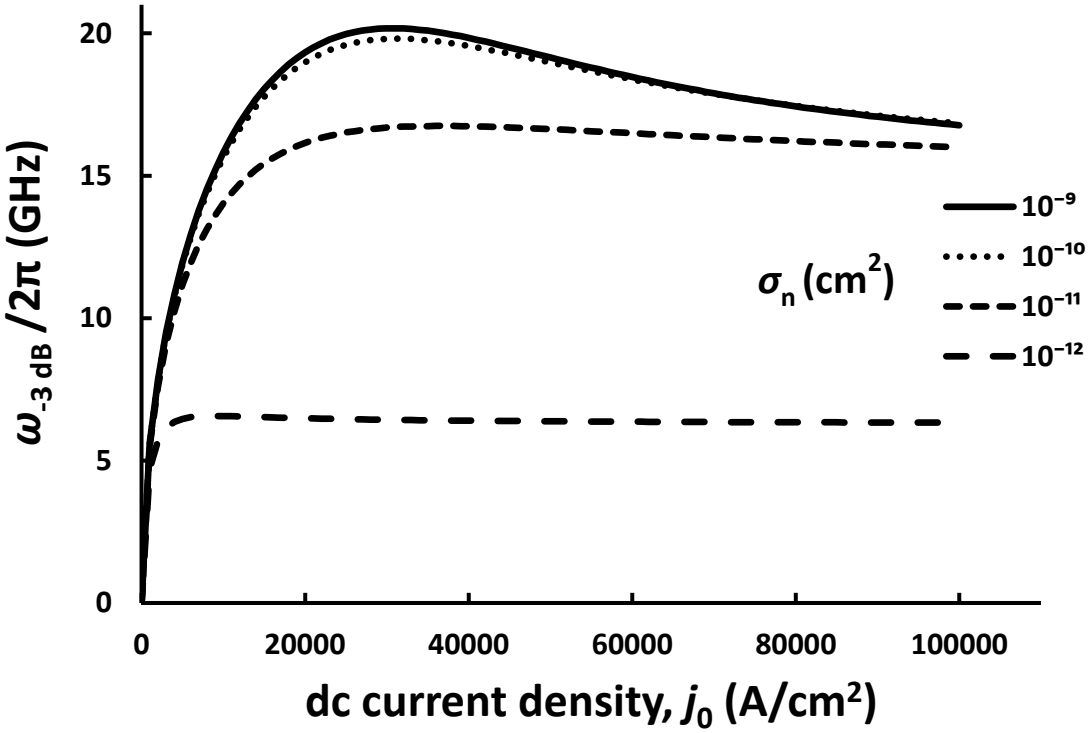

Fig. 7. Modulation bandwidth (GHz) vs dc current density (A/cm^2) with varying cross section of carrier capture (cm^2).

As shown in figure 7, at a specific current density, the bandwidth increases and finally asymptotically approaches its value corresponding to the case of instantaneous capture into QDs [33].

In order to explore how maximum modulation bandwidth increases with increasing cross section of carrier capture, the following graph was created, as shown in Figure 8.

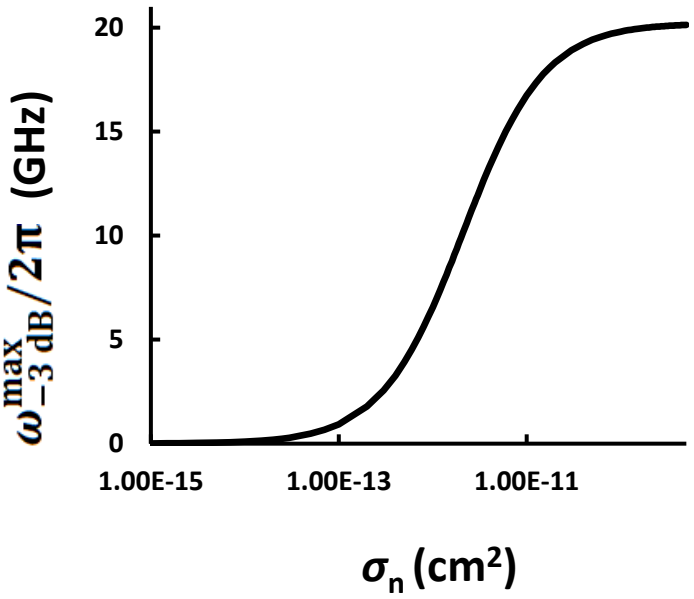

Fig. 8. Maximum modulation bandwidth (GHz) vs cross section of carrier capture (cm^2).

As shown in figure 8, as the cross section of carrier capture gets larger, the maximum modulation bandwidth increases to an asymptotic value of 20 GHz. Thus, when fabricating ABL QDLs, one should strive to have the largest cross section of carrier capture possible. However, once your cross section of carrier capture gets too large, there is no longer any benefit to the larger carrier capture. The modulation bandwidth begins at zero because if no electrons are

captured, lasing does not occur. Once carrier capture hits a certain point, the modulation bandwidth does not change considerably because all the electrons are properly being captured by the QDs, and the laser is operating optimally.

In figure 9, modulation bandwidth was plotted with varying cross section of carrier capture, and with different injection currents.

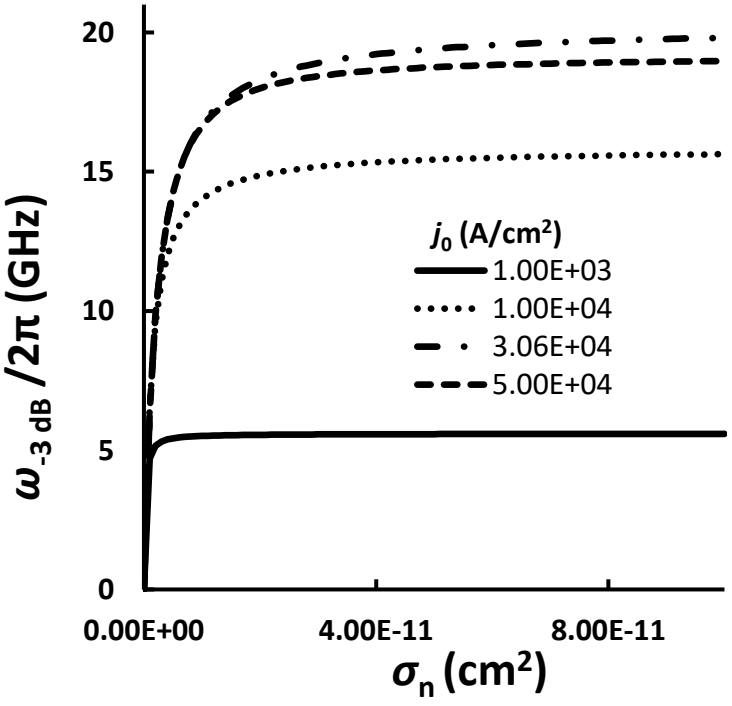

Fig. 9. Modulation bandwidth vs cross section of carrier capture, with varying injection current.

As shown in figure 9, the optimal injection current to maximize modulation bandwidth is 30.61 kA/cm^2. At injection currents lower than the optimal value, the modulation bandwidth achievable is much lower than the value at the optimum value. The modulation bandwidth

increases as the optimum injection current is approached, and drops lower again once the optimum injection current is passed.

2.4.3. Modulation Bandwidth vs Surface Density of QDs

Another parameter tested for was surface density of QDs. This was defined as the amount of QDs per centimeter squared. Figure 10 shows our findings.

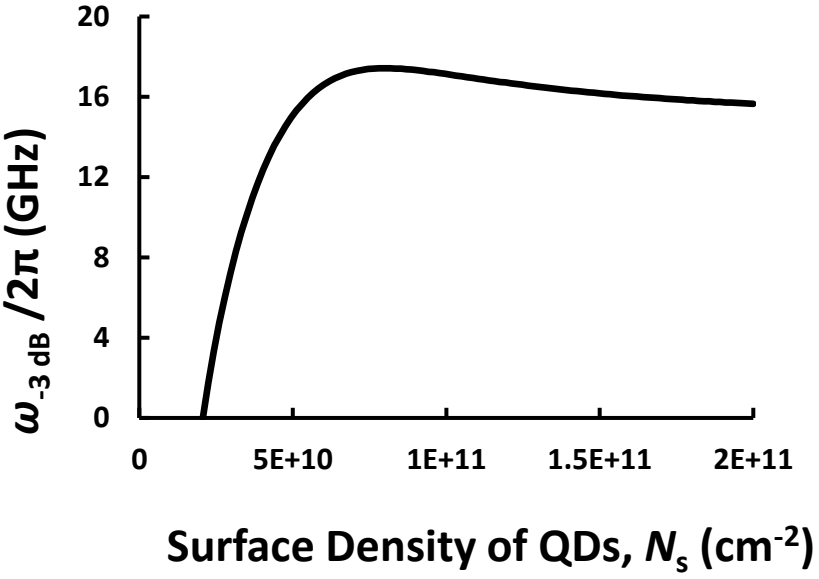

Fig. 10. Modulation bandwidth (GHz) vs surface density of QDs (cm^{-2}).

As shown in Fig 10, modulation bandwidth increases with surface density of QDs, until reaching a maximum value and lowering towards an asymptotic value. Thus, the optimal density of QDs exists.

2.4.4. Modulation Bandwidth vs Cavity Length

The dependence of the modulation bandwidth on the cavity length of the laser was investigated and plotted in Figure 11.

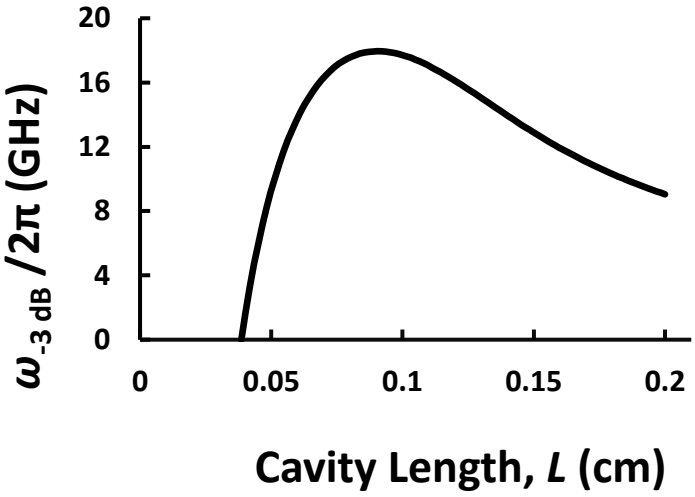

Fig. 11. Modulation bandwidth (GHz) vs cavity length (cm).

As shown in figure 11, modulation bandwidth does not exist until the cavity length is at least 386 μm. Once the cavity is long enough to achieve lasing, the modulation bandwidth increases to a maximum, before dropping to a lower value as the cavity length continues to increase. This mirrors [35], where a minimum cavity length also existed. An optimum cavity length also existed in [35], where the effect of the internal optical loss on the modulation bandwidth was studied.

2.4.5. Modulation Bandwidth vs Root Means Square (RMS) of QD-Size Fluctuations.

While QDs are only a few nanometers in diameter, size variation is inevitable when fabricated. Thus, QD size fluctuation was accounted for in this research. Figure 12 below shows us the modulation bandwidth of the ABL QDL versus RMS of relative QD size fluctuations.

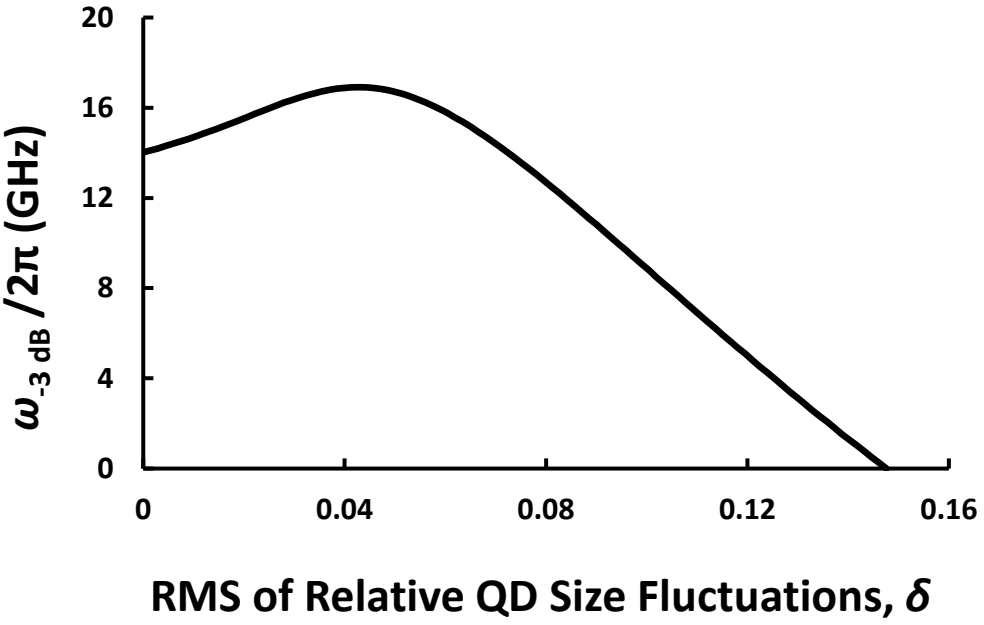

Fig. 12. Modulation bandwidth (GHz) vs RMS of relative QD size fluctuations.

As shown in Fig 12, a slight increase in the size fluctuations of QDs is actually beneficial to the maximum modulation bandwidth of the ABL QDLs, as with a RMS of 0.05, the maximum modulation bandwidth of the system increases by roughly 2.5 GHz. However, if the QD size fluctuations get too large, the modulation bandwidth drops to zero. This is due to the fact that if the size fluctuations of the QD increases and approaches a critical value, the maximum value of

the modal gain of a QD laser [see equations (7) and (8)] will become lower than the mirror loss β [see equation 6] and the lasing condition (19) will not be satisfied.

2.5. Summary

In chapter 2, a theoretical model for QD lasers with ABLs was created. These ABLs were positioned to deny carrier escape from the active region into the OCL. By blocking carrier escape from the active region to the OCL, parasitic recombination of carriers outside the active region is eliminated. This design does not hinder the injection of electrons and holes into the QDs, where recombination occurs. In our model, electron-hole symmetry was assumed. The rate equations for the system were then solved for the steady state case. Small signal analysis of the rate equations was then undertaken, in order to study the modulation response of the ABL QD lasers. The resulting cubic equation in terms of ω_{-3dB}^{2} was then solved to model the behavior of ABL QD lasers at varying currents and different laser parameters, including QD surface density, QD size fluctuation, and cavity length. The cross section of carrier capture was also modeled. An optimum value of dc current density, surface density of QDs, cavity length, and QD size fluctuations were all found, which maximized the modulation bandwidth of the QD lasers with ABLs.

Chapter 2 Bibliography

[33] L. V. Asryan and R. A. Suris, “Upper limit for the modulation bandwidth of a quantum dot laser”, Appl. Phys. Lett. 96, 221112 (2010); https://doi.org/10.1063/1.3446968

[34] L.V. Asryan, Yu. Wu and R. A. Suris, “Carrier capture delay and modulation bandwidth in an edge-emitting quantum dot laser”, Appl. Phys. Lett. 98, 131108 (2011); https://doi.org/10.1063/1.3571295

[35] Yu. Wu, R. A. Suris, and L.V. Asryan, “Effect of internal optical loss on the modulation bandwidth of a quantum dot laser”, Appl. Phys. Lett. 100, 131106 (2012); http://dx.doi.org/10.1063/1.3697683

Chapter 3. Excited States in Quantum Dots

When a carrier is injected into the QD, there is a possibility for the carrier to be captured into an excited state, rather than the ground state. It would be desirable if QDs would contain only one electron and only one hole energy state. However, large and/or deep enough QDs contain excited states as well. Multiple excited states can exist in each of the conduction and valence bands, and can each hold a charge carrier [36-39]. Carriers can recombine through excited states in addition to recombination through the ground state, as shown in figure 13.

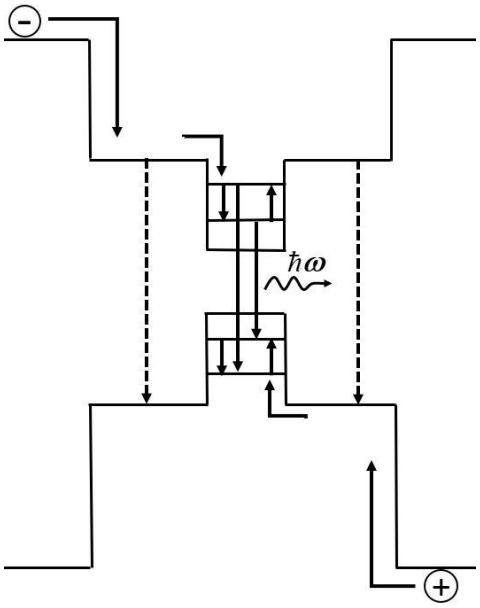

Fig. 13. Energy band diagram of a conventional QD laser.

These excited states can affect the carrier capture from the OCL into the lasing ground state in a QD. If the carrier capture into the QD ground-state takes places via the excited-states,

the emitted power of ground-state lasing eventually reaches an asymptotic value rather than continues to increase with increasing pump current in a conventional QD lasers [36].

By introducing ABLs as before, the electrons and holes will not be able to escape from the active region into the OCL. In figure 14, the energy band diagram and the main processes in an ABL QD laser are shown.

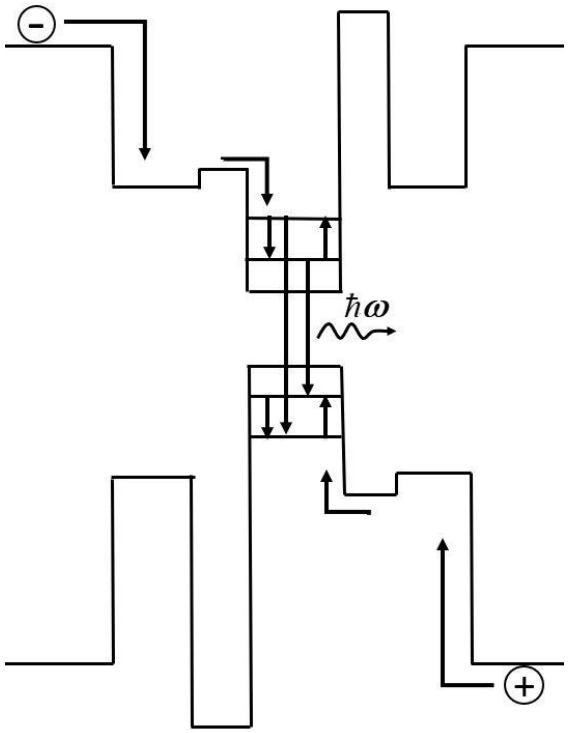

Fig. 14. Energy band diagram of ABL QD lasers.

3.1. Excited-State-Mediated Capture into Ground State in ABL QD Lasers

By assuming electron-hole symmetry, we can use the following set of four rate equations:

for free carriers (electrons) in the left-hand side of the OCL,

$$b_1 \frac{\partial n_{\mathrm{L}}}{\partial t} = \frac{j}{e} + \sigma_{\mathrm{n2}} \mathrm{v}_{\mathrm{n}} n_1 N_{\mathrm{S}} f_{\mathrm{n2}} - \sigma_{\mathrm{n2}} \mathrm{v}_{\mathrm{n}} n_{\mathrm{L}} N_{\mathrm{S}} (1 - f_{\mathrm{n2}}), \quad (93)$$

for carriers confined in the excited states of the QDs:

$$2N_{\mathrm{S}} \frac{\partial f_{\mathrm{n2}}}{\partial t} = \sigma_{\mathrm{n2}} \mathrm{v}_{\mathrm{n}} n_{\mathrm{L}} N_{\mathrm{S}} (1 - f_{\mathrm{n2}}) - \sigma_{\mathrm{n2}} \mathrm{v}_{\mathrm{n}} n_1 N_{\mathrm{S}} f_{\mathrm{n2}} + N_{\mathrm{S}} \frac{f_{\mathrm{n1}}(1 - f_{\mathrm{n2}})}{\tau_{12}} - N_{\mathrm{S}} \frac{f_{\mathrm{n2}}(1 - f_{\mathrm{n1}})}{\tau_{21}} - N_{\mathrm{S}} \frac{f_{\mathrm{n2}}^2}{\tau_{\mathrm{QD2}}} \quad (94)$$

for carriers confined in the ground state in QDs:

$$2N_{\mathrm{S}} \frac{\partial f_{\mathrm{n1}}}{\partial t} = N_{\mathrm{S}} \frac{f_{\mathrm{n2}}(1 - f_{\mathrm{n1}})}{\tau_{21}} - N_{\mathrm{S}} \frac{f_{\mathrm{n1}}(1 - f_{\mathrm{n2}})}{\tau_{12}} - N_{\mathrm{S}} \frac{f_{\mathrm{n1}}^2}{\tau_{\mathrm{QD1}}} - c_{\mathrm{g}} g_1^{\max} (2 f_{\mathrm{n1}} - 1) n_{\mathrm{ph1}}, \quad (95)$$

and for stimulated photons emitted via the ground-state transitions in QDs,

$$\frac{\partial n_{\mathrm{ph1}}}{\partial t} = c_{\mathrm{g}} g_1^{\max} (2 f_{\mathrm{n1}} - 1) n_{\mathrm{ph1}} - c_{\mathrm{g}} \beta_1 n_{\mathrm{ph1}}. \quad (96)$$

At steady-state, eqs. (93)-(96) become

$$0 = \frac{j}{e} + \sigma_{\mathrm{n2}} \mathrm{v}_{\mathrm{n}} n_1 N_{\mathrm{S}} f_{\mathrm{n2}} - \sigma_{\mathrm{n2}} \mathrm{v}_{\mathrm{n}} n_{\mathrm{L}} N_{\mathrm{S}} (1 - f_{\mathrm{n2}}), \quad (97)$$

$$0 = \sigma_{\mathrm{n2}} \mathrm{v}_{\mathrm{n}} n_{\mathrm{L}} N_{\mathrm{S}} (1 - f_{\mathrm{n2}}) - \sigma_{\mathrm{n2}} \mathrm{v}_{\mathrm{n}} n_1 N_{\mathrm{S}} f_{\mathrm{n2}} + N_{\mathrm{S}} \frac{f_{\mathrm{n1}}(1 - f_{\mathrm{n2}})}{\tau_{12}} - N_{\mathrm{S}} \frac{f_{\mathrm{n2}}(1 - f_{\mathrm{n1}})}{\tau_{21}} - N_{\mathrm{S}} \frac{f_{\mathrm{n2}}^2}{\tau_{\mathrm{QD2}}}, \quad (98)$$

$$0 = N_{\mathrm{S}} \frac{f_{\mathrm{n2}}(1 - f_{\mathrm{n1}})}{\tau_{21}} - N_{\mathrm{S}} \frac{f_{\mathrm{n1}}(1 - f_{\mathrm{n2}})}{\tau_{12}} - N_{\mathrm{S}} \frac{f_{\mathrm{n1}}^2}{\tau_{\mathrm{QD1}}} - c_{\mathrm{g}} g_1^{\max} (2 f_{\mathrm{n1}} - 1) n_{\mathrm{ph1}}, \quad (99)$$

$$0 = c_{\mathrm{g}} g_1^{\max} (2 f_{\mathrm{n1}} - 1) n_{\mathrm{ph1}} - c_{\mathrm{g}} \beta_1 n_{\mathrm{ph1}}. \quad (100)$$

In order to have $n_{\mathrm{ph1}} \neq 0$, the following lasing condition was found from (100):

$$g_1^{\max} (2 f_{\mathrm{n1}} - 1) = \beta_1. \quad (101)$$

From (101), the ground-state level occupancy is found:

$$f_{\mathrm{n1}} = \frac{1}{2}\left(1 + \frac{\beta_1}{g_1^{\max}}\right). \tag{102}$$

The output optical power produced by stimulated emission via the ground-state transitions in QDs is

$$P_1 = \hbar\omega_1 c_{\mathrm{g}} \beta_1 n_{\mathrm{ph1}} S = \hbar\omega_1 \frac{n_{\mathrm{ph1}}}{\tau_{\mathrm{ph1}}} S\,, \tag{103}$$

where the photon lifetime in cavity is introduced as

$$\tau_{\mathrm{ph1}} = \frac{1}{c_{\mathrm{g}} \beta_1}\,. \tag{104}$$

Adding up (97) and (98), we found

$$0 = \frac{j}{e} + N_s \frac{f_{n1}(1-f_{n2})}{\tau_{12}} - N_s \frac{f_{n2}(1-f_{n1})}{\tau_{21}} - N_s \frac{f_{n2}^2}{\tau_{QD2}} \tag{105}$$

Rewriting, we get

$$\frac{f_{n2}^2}{\tau_{QD2}} + \frac{f_{n2}(1-f_{n1})}{\tau_{21}} - \frac{f_{n1}(1-f_{n2})}{\tau_{12}} - \frac{j}{eN_s} = 0 \tag{106}$$

which can once again be rewritten to

$$\frac{f_{n2}^2}{\tau_{QD2}} + \left[\frac{(1-f_{n1})}{\tau_{21}} + \frac{f_{n1}}{\tau_{12}}\right] f_{n2} - \left(\frac{f_{n1}}{\tau_{12}} + \frac{j}{eN_s}\right) = 0 \tag{107}$$

Substituting in the following variables, we see

$$a f_{n2}^2 + b f_{n2} + c = 0 \tag{108}$$

$$f_{n2} = \frac{-b \pm \sqrt{b^2 - 4ac}}{2a} \tag{109}$$

$$a = \frac{1}{\tau_{QD2}} \tag{110}$$

$$b = \frac{(1 - f_{n1})}{\tau_{21}} + \frac{f_{n1}}{\tau_{12}} \tag{111}$$

$$c = -\left(\frac{f_{n1}}{\tau_{12}} + \frac{j}{eN_s}\right) \tag{112}$$

Solving the quadratic equation (108) using equations (109)-(112), we begin with

$$b^2 - 4ac = \left(\frac{(1 - f_{n1})}{\tau_{21}} + \frac{f_{n1}}{\tau_{12}}\right)^2 + \frac{4}{\tau_{QD2}}\left(\frac{f_{n1}}{\tau_{12}} + \frac{j}{eN_s}\right) \tag{113}$$

Because b > 0 (eq. 111), the negative solution of the quadratic equation (eq. 109) is a negative value, and thus is dropped (as negative f_{n2} is impossible). Hence, we have

$$f_{n2}(j) = \frac{\tau_{QD2}}{2}\left[\sqrt{\left(\frac{(1 - f_{n1})}{\tau_{21}} + \frac{f_{n1}}{\tau_{12}}\right)^2 + \frac{4}{\tau_{QD2}}\left(\frac{f_{n1}}{\tau_{12}} + \frac{j}{eN_s}\right)} - \left(\frac{(1 - f_{n1})}{\tau_{21}} + \frac{f_{n1}}{\tau_{12}}\right)\right] \tag{114}$$

As shown in (114), f_{n2} increases with increasing *j*. However, f_{n2} cannot exceed one. Hence, (114) applies for the currents

$$j_{th1} \leq j \leq j_2 \tag{115}$$

where j_{th1} is the threshold current density for lasing through the ground state, and j_2 follows the condition

$$f_{n2}(j_2) = 1 \tag{116}$$

Using (114) or (107) (where f_{n2} is set equal to 1), we obtain

$$\frac{1}{\tau_{QD2}} + \frac{(1-f_{n1})}{\tau_{21}} + \frac{f_{n1}}{\tau_{12}} = \frac{f_{n1}}{\tau_{12}} + \frac{j_2}{eN_s} \tag{117}$$

From this, we have

$$j_2 = eN_s\left(\frac{1}{\tau_{QD2}} + \frac{(1-f_{n1})}{\tau_{21}}\right) \tag{118}$$

Hence, for $j_{th1} \le j \le j_2$, f_{n2} is given by (114); for $j \ge j_2$,

$$f_{n2} = 1 \tag{119}$$

From eq. (100) we have

$$\sigma_{n2} v_n n_L N_s (1-f_{n2}) = \frac{j}{e} + \sigma_{n2} v_n n_1 N_s f_{n2} \tag{120}$$

Thus, for n_L, we have

$$n_L(j) = n_1 \frac{f_{n2}(j)}{1-f_{n2}(j)} + \frac{j}{e\sigma_{n2} v_n N_s (1-f_{n2}(j))}. \tag{121}$$

Adding up equations (97), (98), and (99), we have

$$\frac{j}{e} = N_s \frac{f_{n2}^2(j)}{\tau_{QD2}} + N_s \frac{f_{n1}^2}{\tau_{QD1}} + c_g \beta_1 n_{ph1}. \tag{122}$$

In the last term in the right-hand side of (122), we used equation (101).

Using equation (104) for τ_{ph1}, we have

$$\frac{j}{e} = N_s \frac{f_{n2}^2(j)}{\tau_{QD2}} + N_s \frac{f_{n1}^2}{\tau_{QD1}} + \frac{n_{ph1}}{\tau_{ph1}} \tag{123}$$

Rearranging (123), we have

$$n_{ph1}(j) = \tau_{ph1}\left[\frac{j}{e} - \frac{N_s f_{n2}^2(j)}{\tau_{QD2}} - N_s \frac{f_{n1}^2}{\tau_{QD1}}\right] \tag{124}$$

for $j < j_2$. However, when $j > j_2, f_{n2} = 1$ and we have

$$n_{ph1}(j) = \tau_{ph1}\left[\frac{j}{e} - \frac{N_s}{\tau_{QD2}} - N_s\frac{f_{n1}^2}{\tau_{QD1}}\right] \tag{125}$$

For the output power of lasing in the ground-state transitions when $j < j_2$, we have

$$P_1 = \hbar\omega_1 c_g \beta_1 n_{ph1} S = \hbar\omega_1 \frac{n_{ph1}}{\tau_{ph1}} S = \hbar\omega_1 \left[\frac{j}{e} - \frac{N_s f_{n2}^2(j)}{\tau_{QD2}} - N_s\frac{f_{n1}^2}{\tau_{QD1}}\right] S. \tag{126}$$

When $j > j_2$,

$$P_1 = \hbar\omega_1 c_g \beta_1 n_{ph1} S = \hbar\omega_1 \frac{n_{ph1}}{\tau_{ph1}} S = \hbar\omega_1 \left[\frac{j}{e} - \frac{N_s}{\tau_{QD2}} - N_s\frac{f_{n1}^2}{\tau_{QD1}}\right] S. \tag{127}$$

We then found the threshold current density for ground-state lasing by setting $n_{ph1} = 0$ in equation (123) and using the f_{n2} value given by equation (114) [where $j = j_{th1}$]. We arrived at the following equation:

$$j_{th1} = eN_s\frac{f_{n2}^2(j_{th1})}{\tau_{QD2}} + eN_s\frac{f_{n1}^2}{\tau_{QD1}} \tag{128}$$

Equation (128) could then be solved for j_{th1}. However, it is much simpler to find j_{th1} a different way. Setting $n_{ph1} = 0$ in equation (99), we found

$$0 = N_s\frac{f_{n2}(j_{th1})(1 - f_{n1})}{\tau_{21}} - N_s\frac{f_{n1}\left(1 - f_{n2}(j_{th1})\right)}{\tau_{12}} - N_s\frac{f_{n1}^2}{\tau_{QD1}} \tag{129}$$

From this equation, we found

$$\left[\frac{(1 - f_{n1})}{\tau_{21}} + \frac{f_{n1}}{\tau_{12}}\right] f_{n2}(j_{th1}) = \frac{f_{n1}}{\tau_{12}} + \frac{f_{n1}^2}{\tau_{QD1}} \tag{130}$$

Hence, we have

$$f_{n2}(j_{th1}) = \frac{\frac{f_{n1}}{\tau_{12}} + \frac{f_{n1}^2}{\tau_{QD1}}}{\frac{(1-f_{n1})}{\tau_{21}} + \frac{f_{n1}}{\tau_{12}}} \tag{131}$$

Using (131) in (128), we had

$$j_{th1} = \frac{eN_s}{\tau_{QD2}} \left(\frac{\frac{f_{n1}}{\tau_{12}} + \frac{f_{n1}^2}{\tau_{QD1}}}{\frac{(1-f_{n1})}{\tau_{21}} + \frac{f_{n1}}{\tau_{12}}} \right)^2 + \frac{eN_s}{\tau_{QD1}} f_{n1}^2 \tag{132}$$

As seen from (121), for $j \geq j_2$, when $f_{n2} = 1$,

$$n_L = \infty \tag{133}$$

The model used here does not consider the fact that at some current density j_{th2}, stimulated recombination via the excited-states will turn on and for $j > j_{th2}$ there will be both ground-state and excited-state lasing. When this is taken into account, f_{n2} will not increase to 1 with increasing *j.* Instead, it will increase up to

$$f_{n2}(j_{th2}) \equiv f_{n2,th2} < 1 \tag{134}$$

and then will remain pinned with increasing *j*. Hence, n_L will not be infinitely high. We however did not include this into our model.

3.2. Ground-state-lasing power against pump current

The output power versus excess injection current density in conventional QD lasers is shown below in figure 15.

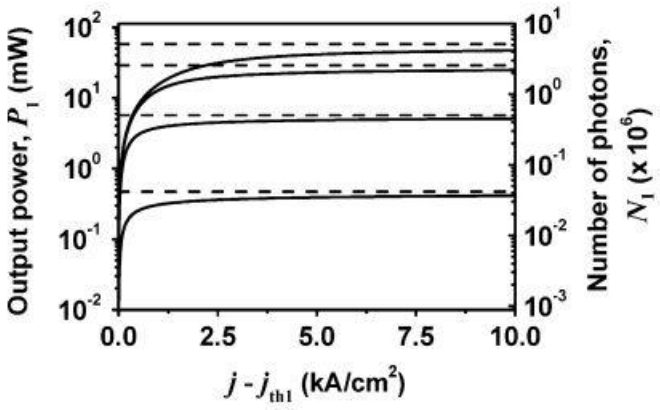

Fig. 15. Output power P_1 (left axis) and number of photons N_1 (right axis) of ground-state lasing versus excess injection current density in conventional QD lasers. The horizontal dashed line shows P_1^{max} and N_1^{max}. Each solid line has a different transition time between excited and ground states. From top to bottom, 1, 2, 10, and 100 ps respectively. [36] © [2006] IEEE

At the lasing threshold ($j = j_{th1}$), the output power is zero (Fig. 15). The output power asymptotically approaches a maximum as current density increases. This is due to the fact that the parasitic recombination in the OCL continuously increases with increasing pump current.

Figure 16 below shows the ground-state-lasing power against excess pump current in QD lasers with ABLs.

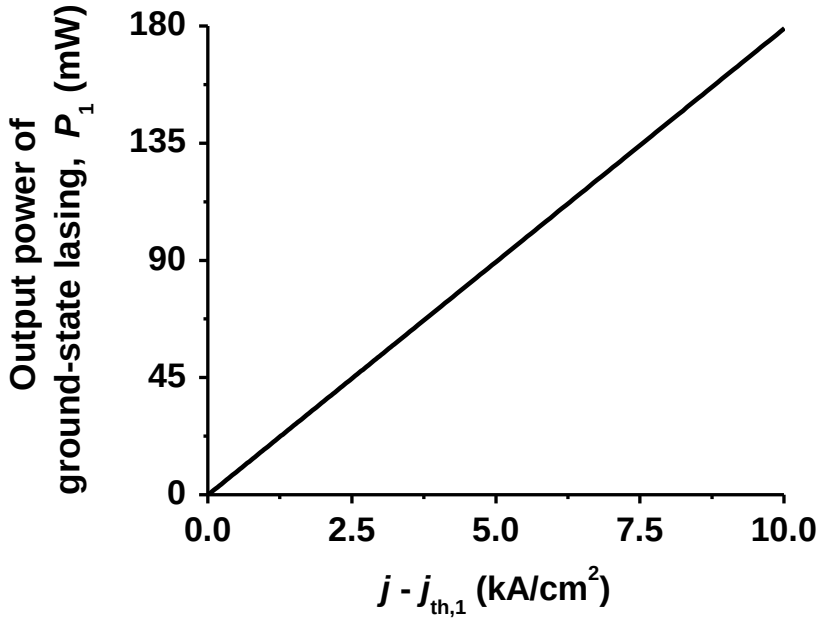

Fig. 16. Output power of ground-state lasing vs excess injection current in ABL QD lasers.

As shown in figure 16, when ABL QD lasers are used, the ground-state lasing power continues to grow as more injection current is applied to the system. This is due to the fact that the ABLs suppress parasitic recombination in the OCL. Thusly, output power will not reach a maximum value as current is applied, and semiconductor QD lasers with ABLs will be able to be applied in systems that required greater output powers.

3.4. Summary

In chapter 3, the output power of ground-state lasing of ABL QD lasers was examined in the presence of excited states in QDs. In ABL QD lasers, by preventing carriers from escaping into

the OCL, parasitic recombination was eliminated from the system. In conventional QD lasers, the output power of ground-state lasing reaches an asymptotic value as pump current increases.

A theoretical model for QD lasers with ABLs was created, which considered excited state mediated capture of carriers into the QD ground state.

It was found that in ABL QD lasers, the output power of ground-state lasing will not reach an asymptotic value with increasing pump current. Rather, the output-power of ground state lasing will continue to increase linearly. This allows QD lasers with ABLs to be used in applications which require high output power.

Chapter 3 Bibliography

[36] L. Jiang and L.V. Asryan, “Excited-state-mediated capture of carriers into the ground state and the saturation of optical power in quantum-dot lasers’, IEEE Photonics Technology Letters, vol. 18, no. 24, pp. 2611-2613, Dec. 2006.

[37] T. Kitamura, R. Ohtsubo, M. Murayama, T. Kuroda, K. Yamaguchi, and A. Tackeuchi, “Direct observation of phonon relaxation bottleneck in InAs quantum dots of high-uniformity,” Phys. Stat. Sol. C, vol. 0, no. 4, pp. 1165–1168, June 2003.

[38] Y. Wu and L.V. Asryan, “Direct and indirect capture of carriers into the lasing ground state and the light-current characteristic of quantum dot lasers,” J. Appl. Phys., vol. 115, no. 10, Art. no. 103105, 5 pages, March 2014.

[39] Y. Wu, L. Jiang, and L.V. Asryan, “Output power of a quantum dot laser: Effects of excited states,” J. Appl. Phys., vol. 118, no. 18, Art. no. 183107, 14 pages, Nov. 2015.

Chapter 4: Conclusion

In this research on semiconductor QD lasers, ABLs were designed in order to stop parasitic recombination of carriers outside of the active region. The optimum pump current was found which maximized modulation bandwidth at -3dB, which was lower than that in conventional QD lasers. Optimal values for surface density of QDs and cavity length were found as well. Relative QD size fluctuation was also investigated, and an optimal value was found. This data gives strong parameters for fabricating semiconductor QD lasers with ABLs with the largest possible modulation bandwidth.

Output power of semiconductor QD lasers with ABLs was also investigated. By including ABLs and suppressing parasitic recombination, the output power of ground state lasing will continue to rise with increasing injection current, as opposed to reaching an asymptotic value as occurs in conventional QD lasers. This allows QD lasers with ABLs to be used in systems that require higher power applications.